Summer 2020

Synthesis and Characterization of Starburst Pseudorotaxanes and Their Metallic Derivatives

Shalini D. Kadinappulige
Eastern Illinois University

Synthesis and Characterization of Starburst Pseudorotaxanes and Their Metallic Derivatives

Shalini D. Kadinappulige

To my family

Abstract

Mechanically Interlocked Molecules (MIMs) are interlocked molecular architectures, characterized by the fact that they are linked through a mechanical bond. Catenanes, rotaxanes, molecular knots, and Borromean rings are typical examples for these molecules. Since MIMs are not connected by covalent bonds, hydrogen bonding, π- π stacking, and/or electrostatic interactions help bring the components together. Dialkyl-ammonium centers, bis(pyridinium)ethane dications, viologen species, and naphthalenediimide π-deficient groups are well known as recognition motifs for crown ethers.

In the research described here, we have synthesized several pseudorotaxanes and their tricyclohexyltin metallic derivatives, based on benzobis(imidazolium) (BBI) salts as axles, in combination with the 15DN38C10 crown ether acting as a wheel. These species are characterized by the fact that the benzobis(imidazolium) core is trapped inside the cavity of the crown ether and the four arms of the axle are extending away directly from the cavity of the crown. This produces a straddled orientation of the wheel onto the axle. We named these species starburst [2_4]pseudorotaxanes, where the number 2 represents the number of components of the pseudorotaxane, and the number 4 indicates the number of the arms protruding from the cavity of the crown.

^{1}H-NMR studies showed that the synthesized pseudorotaxanes exhibit a fast exchange on the NMR timescale. In order to calculate the association constant K_a, we performed NMR titrations in acetone-d_6 at 293 K. The chemical shifts of the protons of crown ether were monitored and association constant values were determined using the Bindfit software. The pseudorotaxane based on the metal complex of the axle containing two donor arms showed the highest association constant, followed by the ditopic carboxylate species, while the tetratopic carboxylate species showed the smallest K_a value, in agreement with the hydrogen bonding possibilities of each species. The axle containing four tricyclohexyltin

centers does not form a pseudorotaxane architecture, because the size of the metallic groups prevents the interaction between the axle and the crown.

Solid-state studies performed on one of the prepared species showed that indeed these pseudorotaxanes have the predicted straddled structure. This architecture is held in place by hydrogen bonding, π-π stacking, and several $[N - CH - N]^{+} \cdots O$ ion – dipole interactions. In addition, all carboxylic groups on the BBI core are involved in multiple hydrogen bonding interactions, either among themselves or with solvent molecules, thus confirming our conclusions drawn from our studies on the association constants of the prepared species.

Acknowledgements

I am using this opportunity to thank everyone who supported me in numerous ways to complete my thesis research.

I would like to express my gratitude to Dr. Radu F. Semeniuc, for providing his expert guidance throughout two years as my mentor. He was a great person and a researcher to work with, and he never hesitated to share his knowledge, which made this goal achieved by the time.

I would also like to thank the members of my thesis committee, Dr. Daniel Sheeran, Dr. Zhiqing Yan, and Dr. Michael Beck, for their valuable feedback, availability and expertise in increasing the quality of this thesis.

Additionally, I wish to thank the Donors of the American Chemical Society's Petroleum Research Fund (grant 56706-UR3) for providing the financial support to complete this research.

I am utterly grateful to the EIU Chemistry Department for the excellent facilities and equipment provided to carry out my research work. The faculty and staff of the EIU Chemistry department have been supportive in various ways, to which I am most grateful.

This accomplishment would not have met without the encouragements from my parents, family, and friends.

Table of Contents

Abstract		iii
Acknowledgements		v
Table of Contents		vi
List of Figures		viii
List of Tables		ix
List of Schemes		x
I	Introduction	1
I.1	Mechanically Interlocked Molecules	1
I.1.1	General information about Mechanically Interlocked Molecules (MIMs)	1
I.1.2	Recognition motifs for MIMs formation	2
I.1.3	Molecular motion in MIMs	4
I.1.4	Potential applications of MIMs	5
I.2	Rotaxanes and pseudorotaxanes	6
I.3	Metal Organic Rotaxane Frameworks (MORFs)	10
I.4	Our approach	13
I.5	References	16
II	Experimental	19
II.1	General considerations	19
II.2	Synthesis of the axle components	19
II.2.1	Synthesis of $C_6H_2Cl_2(NO_2)_2$, intermediate A	20
II.2.2	Synthesis of $C_6H_2(NO_2)_2(NHBu)_2$, intermediate B	20
II.2.3	Synthesis of $BBI(Bu)_2$, intermediate C	20
II.2.4	Synthesis of $\{BBI(Bu)_2[(CH_2)_4COOMe]_2\}Br_2$, intermediate D	21
II.2.5	Synthesis of $\{BBI(Bu)_2[(CH_2)_4COOMe]_2\}(PF_6)_2$, intermediate E	21

II.2.6	Synthesis of the {BBI(Bu)$_2$[(CH$_2$)$_4$COOSnCy$_3$]$_2$}(PF$_6$)$_2$ axle, F	22
II.2.7	Synthesis of benzobis(imidazole), intermediate G	22
II.2.8	Synthesis of {BBI[(CH$_2$)$_4$COOH]$_4$}(PF$_6$)$_2$, intermediate I	23
II.2.10	Synthesis of the {BBI[(CH$_2$)$_4$COOSnCy$_3$]$_4$}(PF$_6$)$_2$ axle, J	23
II.3	Synthesis of the bis-1,5-(dinaphtho)-38-crown-10 (15DN38C10) wheel	24
II.3.1	Synthesis of CH$_3$-C$_6$H$_4$-(CH$_2$-CH$_2$-O)$_4$H, intermediate K	24
II.3.2	Synthesis of C$_{10}$H$_6$[(O-CH$_2$-CH$_2$)$_4$-OH]$_2$, intermediate L	25
II.3.3	Synthesis of C$_{10}$H$_6$[(O-CH$_2$-CH$_2$)$_4$-O-C$_6$H$_4$-CH$_3$]$_2$, intermediate M	25
II.3.4	Synthesis of the 15DN38C10 crown ether	26
II.4	NMR titrations	26
II.5	Crystallography	27
II.6	References	28
III	Results and Discussion	30
III.1	Synthetic Considerations	30
III.2	Spectroscopic Characterization	33
III.2.1	Axles characterization	33
III.2.2	Pseudorotaxane characterization	36
III.3	Thermodynamic characterization	37
III.4	Solid state studies	43
III.5	References	47
IV	Conclusions and future work	49
Appendix A		52

List of Figures

Figure I.1.	Cartoon representation of some Mechanically Interlocked Molecules (MIMs): a) catenanes, b) rotaxanes, c) pretzelanes, d) Borromean rings. (Figure from references 3, 4 and 5).	1
Figure I.2.	Molecular motions in rotaxanes: a) ring shuttling and b) ring rotation; c) $CBPQT^{4+}$ ring shuttling under acid / base inputs. (Figure from references 5 and 17).	4
Figure I.3.	Schematics of a) the bistable [2]rotaxanes and the monolayered mechanized silica nano-particles (MSNPs) and b) the proposed mechanism for loading and releasing cycle of cargo molecules. The silica particles are not drawn to scale, and only a few of the ordered pores are shown. (Figure from reference 24).	6
Figure I.4.	Cartoon representation of: a) a pseudorotaxane and b) a rotaxane; c) rotaxane naming details. (Figure from reference 27).	7
Figure I.5.	The threading-followed-by-stoppering (Method A) and the clipping (Method B) strategies used in the synthesis of rotaxanes. (Figure from reference 28).	8
Figure I.6.	The preparation of a [n]rotaxane (n up to 11). (Figure from reference 28).	9
Figure I.7.	The [2]rotaxane studied by David Leigh. (Figure from reference 29).	9
Figure I.8.	Examples of Cu-Based rotaxane and Ln-based rotaxane. (Figure from reference 30).	10
Figure I.9.	Formation of 1D, 2D and 3D MORFs using a [2]pseudorotaxane as a linker. (Figure from reference 32).	11
Figure I.10.	The 1D MORF built by a CB[6] wheel, a N,N'-bis(4-pyridylmethyl)-1,4-diaminobutane axle, and $Cu(NO_3)_2$ nodes. (Figure from reference 33).	12
Figure I.11.	Ball and stick representation of the repeating unit in $\{[M(H_2O)_2(MeCN)_2[BF_4]_4 \cdot (MeCN)_2 \cdot (H_2O)_2\}_x$; Color code: blue – axle, red – DB24C8, dark blue – metal ion, yellow – MeCN, green – H_2O. (Figure from reference 34).	13
Figure I.12	Cartoon representations of: a) regular $[2_2]$pseudorotaxanes; and b) starburst $[2_4]$pseudorotaxanes. (Figure from reference 35).	14

Figure III.1.	Partial ^{1}H-NMR spectrum of intermediate **C**, BBI-$(Bu)_2$.	34
Figure III.2.	Partial ^{1}H-NMR spectrum of intermediate **E**, BBI-$(Bu)_2$-$[(CH_2)_4$-$COOH]_2(PF_6)_2$	34
Figure III.3.	Partial ^{1}H-NMR spectrum of the ditopic tricyclohexyltin-based axle **F**.	35
Figure III.4.	Partial ^{1}H-NMR spectrum of intermediate **I**, BBI-$[(CH_2)_4$-$COOH]_4(PF_6)_2$.	35
Figure III.5.	Partial ^{1}H-NMR spectrum of the tetratopic tricyclohexyltin-based axle **J**.	36
Figure III.6.	a) Schematic view of the pseudorotaxanes studied in this work; b) changes in the NMR spectrum after the formation of the BBI$(Bu)_2[(CH_2)_4$-$COOH]_2\subset$15DN38C10 (blue line – bottom) from 15DN38C10 (red line – middle) and BBI$(Bu)_2[(CH_2)_4$-$COOH]_2$ (green line – top); color code: green – axle, red – crown, blue – pseudorotaxane.	37
Figure III.7.	a) The shift of the signals corresponding to the H_b protons in the case of BBI$(Bu)_2[(CH_2)_4$-$COOH]_2\subset$15DN38C10; b) the shift of the signals corresponding to the H_b protons in the case of BBI$(Bu)_2[(CH_2)_4$-COO-$SnCy_3]_2\subset$15DN38C10.	40
Figure III.8.	Titration curves for the pseudorotaxane systems studied in this work	41
Figure III.9.	The structure of the $\{BBI[(CH_2)_4COOH)]_4\subset 15DN38C10\}^{2+}$ assembly: a) side view in ball and stick representation; the blue dashed lines show the H-bonding interactions, and the triple red lines the π-π stacking interactions; b) top view of the interlocked architecture as a space filling representation.	45
Figure III.10.	The supramolecular association of the axle via hydrogen bonding interactions involving the carboxylic groups on the axle	47

List of Tables

Table III.1	Thermodynamic data for the pseudorotaxanes studied in this work.	43
Table III.2	Crystal and refinement data for $\{BBI[(CH_2)_4COOH)]_4\}(PF_6)_2\subset$15DN38C10.	44

Table III.3 Essential non-covalent interactions found in the molecular and crystal structure of $\{BBI[(CH_2)_4COOH)]_4\}(PF_6)_2 \subset 15DN38C10$. 46

List of Schemes

Scheme I.1 Cucurbituril-based interlocked molecules: a) formation of a rotaxane species – the CB moiety is schematically represented by a simplified drawing; b) the structure of CB[6]. (Figure from reference 1). 2

Scheme I.2 Crown ethers and axle components used in the preparation of pseudorotaxanes and rotaxanes. (Figure from reference 16). 3

Scheme I.3. Comparison between a) $[BipyH_2]^{2+}$ and b) $[BBI\text{-}H_2\text{-}R_4]^{2+}$ dications and their interaction with BPP34C10. (Figure from reference 35). 16

Scheme II.1. Reaction pathway for the preparation of the two-arm axle 19

Scheme II.2. Reaction pathway for the preparation of the four-arm axle 22

Scheme II.3. Reaction pathway for the preparation of the 15DN38C10 crown ether 24

Scheme III.1. Reaction steps taken for the preparation of the two-arm axle 31

Scheme III.2. Reaction steps taken for the preparation of the four-arm axle 32

Scheme III.3. Reaction steps taken for the preparation of the 15DNC10 crown ether 32

I. Introduction

I.1. Mechanically Interlocked Molecules

I.1.1. General information about Mechanically Interlocked Molecules (MIMs)

Mechanically Interlocked Molecules (MIMs) have showed a significant development in past few years.[1] These species consist of two or more molecular components that are mechanically interlocked. This means that in order to separate these components, one has to break at least one covalent bond. Typical examples of MIMs are catenanes, rotaxanes, molecular knots, and Borromean rings, pictured in Figure I.1.[2, 3, 4]

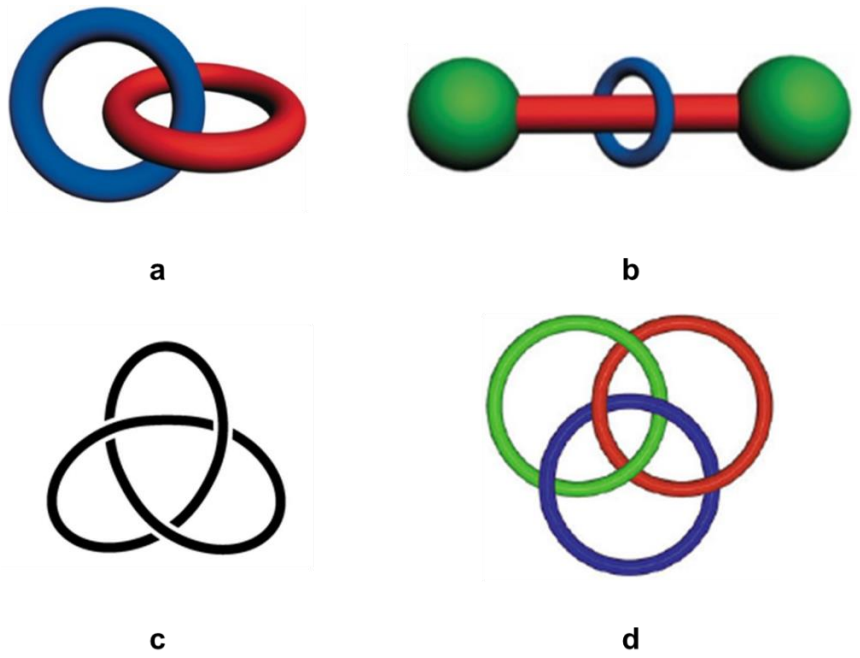

Figure I.1. Cartoon representation of some Mechanically Interlocked Molecules (MIMs): a) catenanes, b) rotaxanes, c) pretzelanes, d) Borromean rings. (Figure from references 3, 4 and 5).

A catenane (Figure I.1.a) is made up from two or more mechanically interlocked macrocycles, while a rotaxane (Figure I.1.b) consists of at least one axle threaded through a macrocycle. Pretzelanes (Figure I.1.c) are similar to catenanes and they have a spacer linking two macrocycles. Three topological rings connecting together make a molecular Borromean ring (Figure I.1.d) and removal of one ring leads to the separation of other two rings as well.[5, 6, 7, 8] As it will be detailed below, the interactions responsible to bring the components together are H- bonding, π- π stacking, and/or electrostatic interactions.

I.1.2. Recognition motifs for MIMs formation

The formation of these species depends on the presence of complementary recognition sites on the components of the assembly. One example of such recognition site is the interaction between cucurbiturils (CBs) and dialkylammonium-based strings, as shown in Scheme I.1.

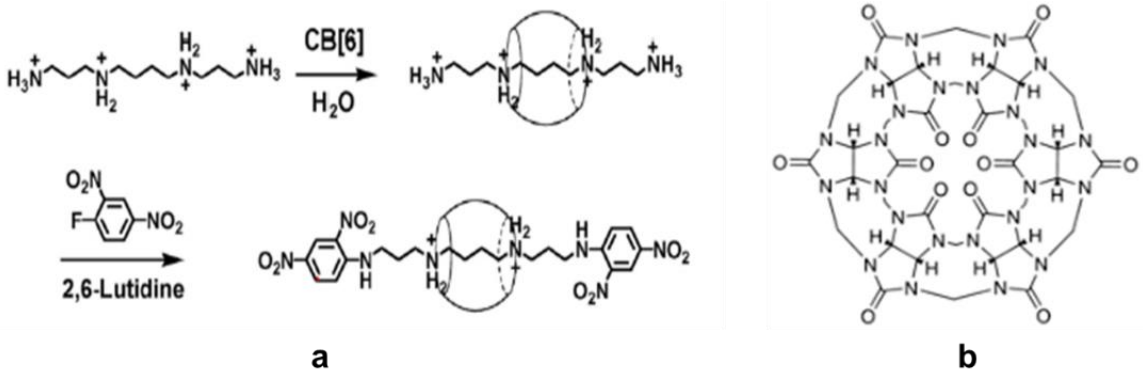

Scheme I.1. Cucurbituril-based interlocked molecules: a) formation of a rotaxane species – the CB moiety is schematically represented by a simplified drawing; b) the structure of CB[6]. (Figure from reference 1).

Another method of preparing rotaxanes in based on the interaction between crown ethers with various linear species. As extensively demonstrated by Stoddart[9, 10] and others[11], a secondary dialkyl-ammonium center (Scheme I.2.a) can be used as a recognition site because it threads into crown ethers like dibenzo-24-crown-8 (DB24C8) and bis-*p*-phenylene-34-crown-10 (BPP34C10) with the formation of (pseudo)rotaxanes. Another set is based on the bis(pyridinium)ethane dication (Scheme I.2.b) and DB24C8, template that was used by Loeb to prepare a large variety of pseudo(rotaxanes).[12] The threading of viologen species (Scheme I.2.c) through the cavities of crown ethers such BPP34C10 and bis-1,5-(dinaphtho)-38-crown-10 (15DN38C10) to form [(viologen)⊂(crown ether)]$^{2+}$ [2]pseudorotaxanes has been studied by Stoddart[13] and others[14] and lies at the foundation of a wide range of MIMs in general, and pseudorotaxane and rotaxane systems, in particular. Sanders showed that rotaxanes can also form from the naphthalenediimide π-deficient group (Scheme I.2.d) and the π-rich 15DN38C10.[15]

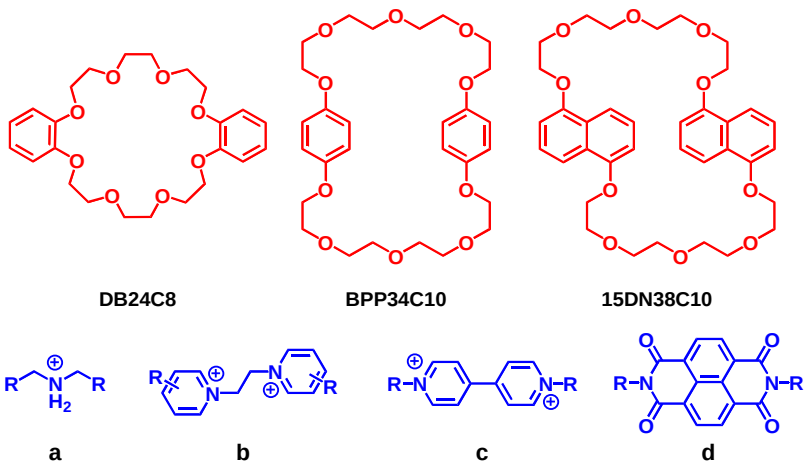

Scheme I.2. Crown ethers and axle components used in the preparation of pseudorotaxanes and rotaxanes. (Figure from reference 16).

I.1.3. Molecular motion in MIMs

Due to the interlocked nature of these species, MIMs have been studied for their possibility to sustain mechanical motion at the molecular scale. In particular, rotaxanes have been studied as molecular shuttles, molecular switches, and molecular machines due to the dynamic ability of the ring to slide along the linear component. The wheel can move from one station to another (ring shuttling, see Figure I.2.a) or circle around the axle (ring rotation, as pictured in Figure I.2.b). These molecular motions can trigger changes in their chemical, photochemical and electrochemical properties. For example, Stoddart studied a molecular shuttle, consisting of a $CBPQT^{4+}$ ring shuttling back and forth between the two hydroquinone units and implemented the shuttling process by changing the pH of the system (Figure I.2.c).

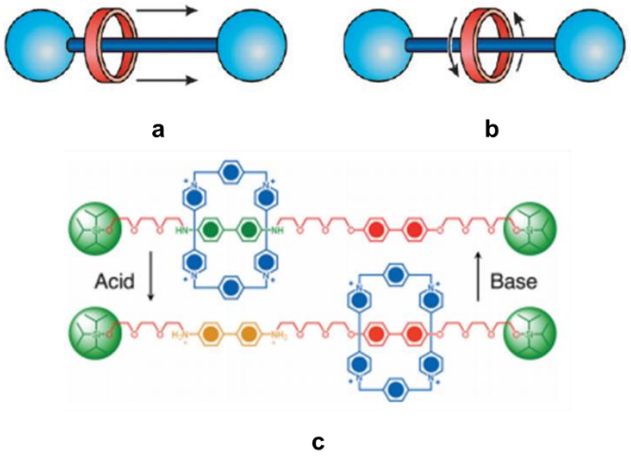

Figure I.2. Molecular motions in rotaxanes: a) ring shuttling and b) ring rotation; c) $CBPQT^{4+}$ ring shuttling under acid / base inputs. (Figure from references 5 and 17).

Other investigations on this topic include the studies of Poleschak, Kern and Sauvage on a redox based molecular machine, while Balzani, Credi and Venturi have done research on photochemical driven molecular machines.[5, 17] The literature contains a multitude of similar studies, and the interested reader can find relevant information on this topic in the "Molecular Machines Special Issue" published in Accounts of Chemical Research, 2001, volume 34(6).

I.1.4. Potential applications of MIMs

The dynamic nature of MIMs prompted a huge number of research groups to study their potential applications in molecular electronics, sensors (e.g. identifying anions in water), and drug delivery. An example for molecular electronics is the crossed bar memory circuit based on a bistable [2]rotaxane described by Stafford and his group. This system is composed of two recognition sites, a tetrathiafulvalene and dioxynapthalene moieties, and a tetracationic $[CBPQT]^{4+}$ wheel.[18, 19]

Paul D. Beer and his research group studied a halogen bonding rotaxane to determine nitrogen-based ions in aqueous medium. Also, they have studied a Ru(II) based rotaxane which senses the iodide anion in water.[20, 21]

Stoddart, Zink and coworkers investigated MIMs as drug delivery systems at a nanoscale. The reported systems have three major units 1) a solid support, b) a payload of cargo (or the therapeutics), and c) the molecular machinery (MIMs). The figure below shows an example for a nano scaled drug delivery system.[22, 23, 24]

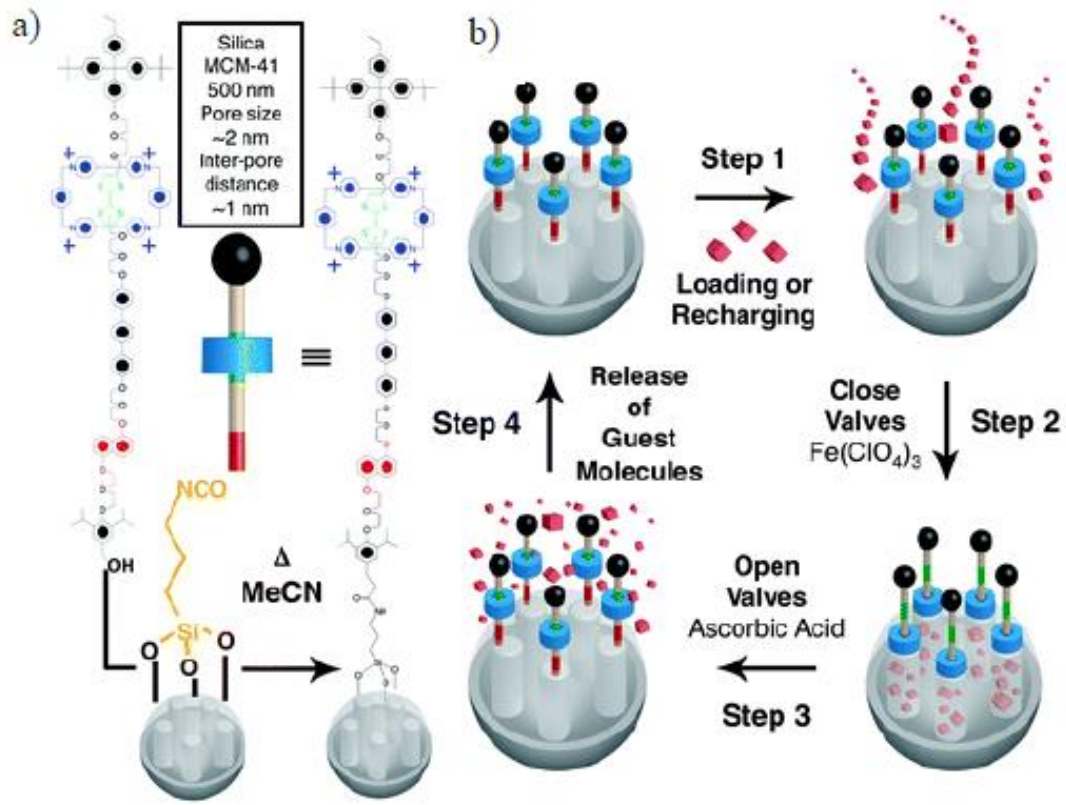

Figure I.3. Schematics of a) the bistable [2]rotaxanes and the monolayered mechanized silica nano-particles (MSNPs) and b) the proposed mechanism for loading and releasing cycle of cargo molecules. The silica particles are not drawn to scale, and only a few of the ordered pores are shown. (Figure from reference 24).

I.2. Rotaxanes and pseudorotaxanes

As mentioned above, the interaction between a linear axle and a cyclic wheel results in the formation of what it is called either a pseudorotaxane or a rotaxane. Their name is derived from “rota” (Latin for wheel) and “ax” from axle. Pseudorotaxanes and rotaxanes consist of one or more macrocycles threaded into one or more axles (linear, dumbbell shaped molecules). Pseudorotaxanes are compounds that exist in equilibrium with their unthreaded

counterparts (the macrocyclic component is free to slip off of the axle); in contrast, rotaxanes are interlocked compounds in which the crown is permanently trapped onto the axle by bulky stoppers at the axle termini[9, 25] (see Figure I.4.a and I.4.b). In naming these compounds, the following notation it is used: *[n]rotaxane*, where the number inside the brackets indicates the total number of components in the rotaxane, as it can be seen in Figure I.4.c.[26, 27]

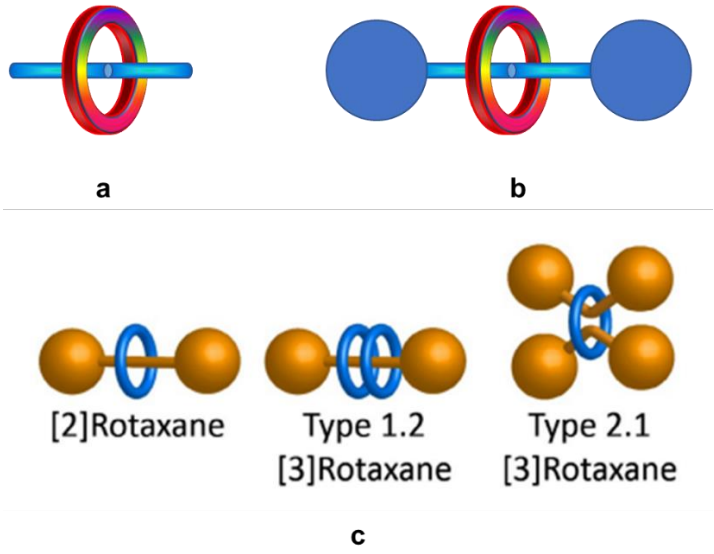

Figure I.4. Cartoon representation of: a) a pseudorotaxane and b) a rotaxane; c) rotaxane naming details. (Figure from reference 27).

Rotaxanes can be prepared using several methods. One method involves the threading of the macrocycle by the axle and then two bulky groups are added at the ends of the axle as stoppers. This method is called “threading-followed-by-stoppering”. The second method is “clipping”. Here, in the presence of the templating recognition sites on the axles,

macrocycles form as acyclic precursors and clip them under thermodynamically controlled conditions.[28] Both these methods are pictured in Figure I.5.

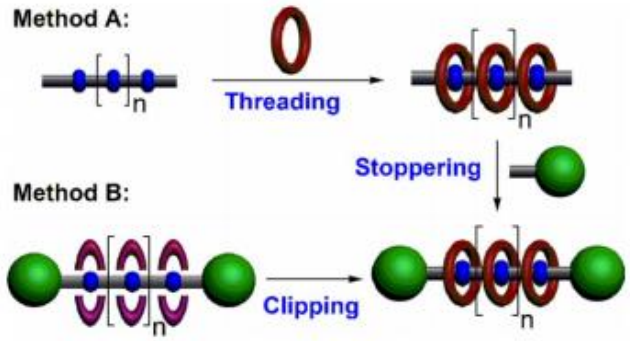

Figure I.5. The threading-followed-by-stoppering (Method A) and the clipping (Method B) strategies used in the synthesis of rotaxanes. (Figure from reference 28).

Many research groups have studies on the rotaxanes, which contain organic components as well as metal-based rotaxanes. Stoddart and his group in 2007 studied a polyrotaxane assembly constructed using the thermodynamically controlled template directed clipping method. They have prepared [n]rotaxanes (with n up to 11) by using dialkylammonium ions ($–CH_2NH_2^+CH_2–$) as recognition sites and 24-crown-8 wheels prepared by the condensation reaction between 2,6-pyridinedicarboxaldehydes and a tetraethyleneglycol bis(2-aminophenyl)ether moiety, see Figure I.6.[28]

Another example of an organic based rotaxane is the [2]rotaxane studied by David Leigh and his research group. The macrocycle contains both H bonding donor and acceptor group[29] , as they are represented in Figure I.7.

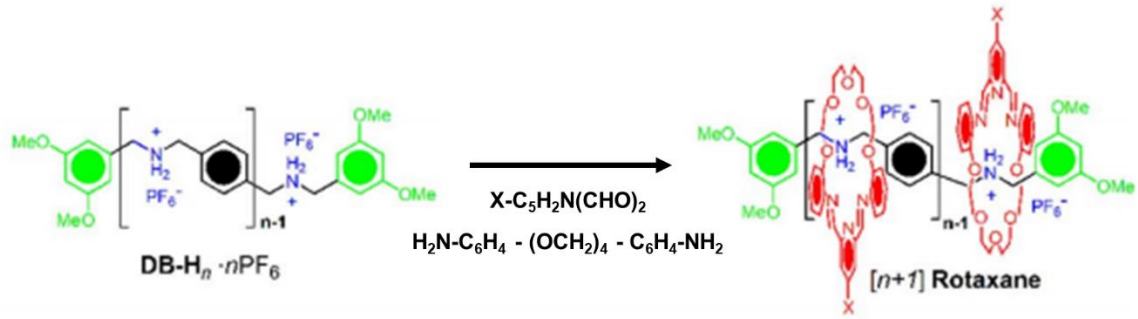

Figure I.6. The preparation of a [n]rotaxane (n up to 11). (Figure from reference 28).

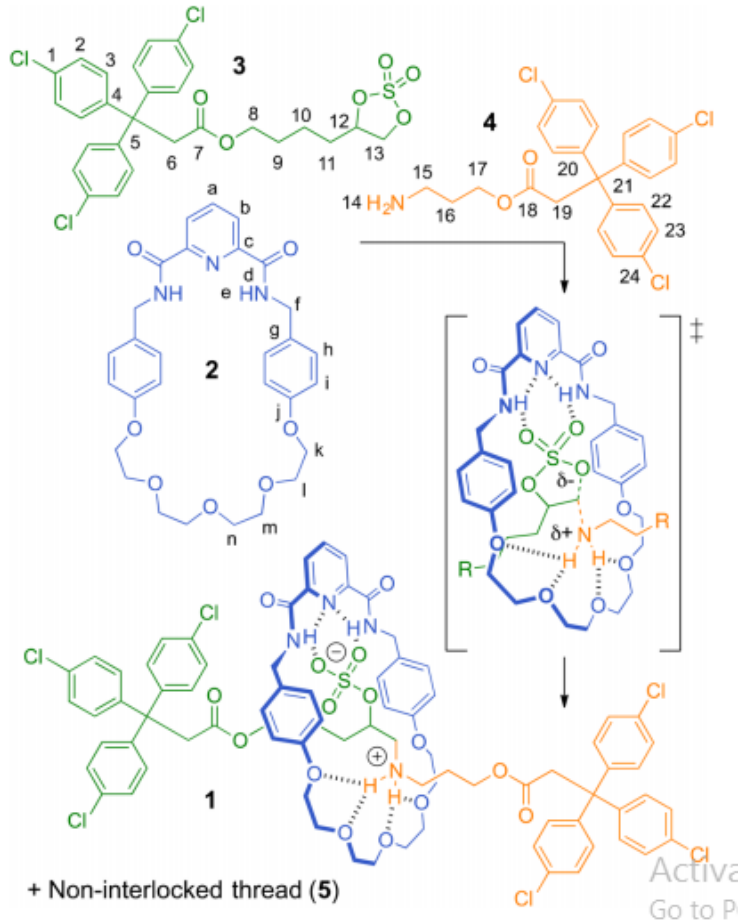

Figure I.7. The [2]rotaxane studied by David Leigh. (Figure from reference 29).

Metallic centers have also been used to prepare rotaxane species, based on their coordination preferences. Figure I.8 shows two such examples, one based on a Cu(I) ion, and the second on a Ln(III) species. It is believed that the presence of metals within the composition of interlocked species will bring within the assembly the interesting electronic, magnetic and catalytic properties of the metals. Beer, Loeb and Goldup have described metal-based rotaxanes in their review article.[30]

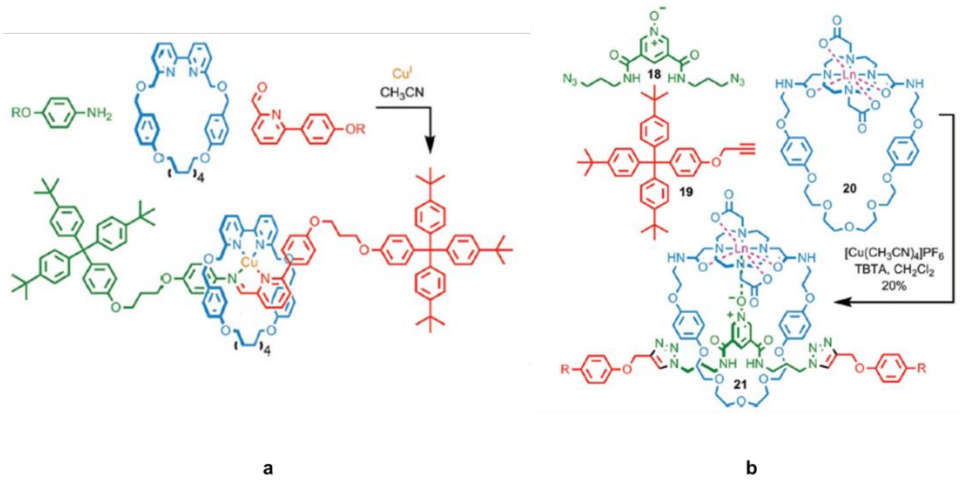

Figure I.8. Examples of Cu-Based rotaxane and Ln-based rotaxane. (Figure from reference 30).

I.3. Metal Organic Rotaxane Frameworks (MORFs)

As mentioned above, an important research direction in this field is the use of (pseudo)rotaxanes as ligands. It is believed that the incorporation of metals in the interlocked architecture would lead to a synergistic effect, thus enhancing the properties of

the resulting interlocked species. As such, several metal-containing interlocked architectures have been prepared and characterized.[15,25] Usually, their design is based on an axle having a recognition site for pseudorotaxane formation and equipped with donor groups for subsequent coordination to metallic centers. The resulting species could provide a blueprint for the future organization of more complex species into higher-order arrays, thus generating crystalline materials comprised of interlocked molecular components that could be independently manipulated.[12] These species are known as Metal Organic Rotaxane Frameworks, or MORFs for short. Kimoon Kim, Stephen Loeb, Jonathan Sessler, and Fraser Stoddart and their research groups have studied and reported several examples of MORFs.[31] The selection of the donor atoms at the ends of pseudorotaxane linkers, the nature of the solvent (coordinating or noncoordinating), metal ions and counter-ions are very important factors that determine the formation and the dimensionality of these MORFs, i.e. mono-, bi- and tri-dimensional networks (see Figure I.8.).[32]

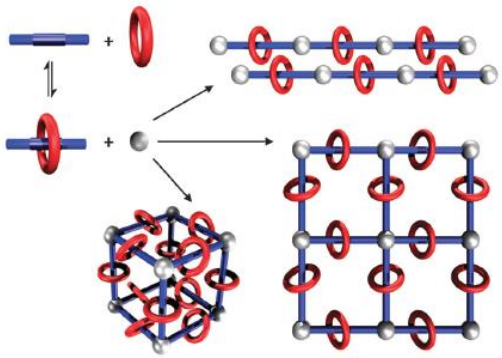

Figure I.9. Formation of 1D, 2D and 3D MORFs using a [2]pseudorotaxane as a linker. (Figure from reference 32).

The studies of Kimoon Kim and his colleagues starting in 1996 made use of various combinations between the highly symmetric CB[6] as the wheel component and diamino alkane derivatives as axles to build the required [2]pseudorotaxanes. Since transition metals have the ability to make relatively strong bonds and they have preferred coordination geometries, they have been used as metallic centers to build 1D, 2D, and / or 3D MORFs. One of the first example of a 1D network consists of a CB[6] wheel and a N,N'-bis(4-pyridylmethyl)-1,4-diaminobutane as an axle, and results in the formation of a [2]pseudorotaxane. The reaction between this pseudorotaxane and $Cu(NO_3)_2$ form the 1D MORF. The process is represented in Figure I.9.[33]

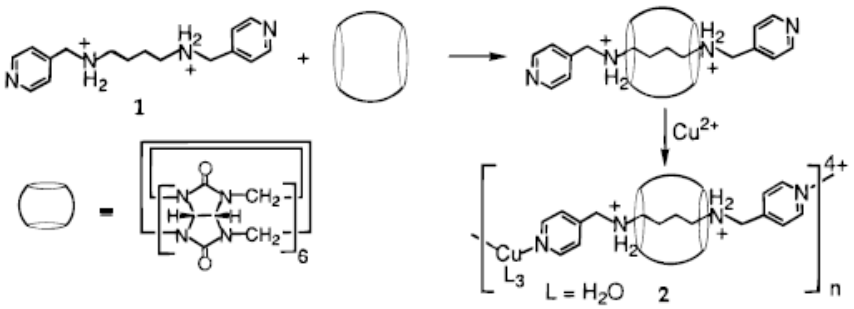

Figure I.10. The 1D MORF built by a CB[6] wheel, a N,N'-bis(4-pyridylmethyl)-1,4-diaminobutane axle, and $Cu(NO_3)_2$ nodes. (Figure from reference 33).

Another example consists in Stephen Loeb's 1D metal-organic-rotaxane-framework prepared by mixing the 1,2-bis(4,4'-bipyridinium)ethane dication with 2 times excess of DB24C8 in MeCN solution, to form the initial pseudorotaxane component. Then, upon the reaction of this species with $[M(H_2O)_6](BF_4)_2$ metal-based starting materials (M = Co, Zn)

the 1D MORF having the formula $\{[M(H_2O)_2(MeCN)_2[BF_4]_4\cdot(MeCN)_2\cdot(H_2O)_2\}_x$ (see Figure I.9.) was obtained.[34]

Figure I.11. Ball and stick representation of the repeating unit in $\{[M(H_2O)_2(MeCN)_2[BF_4]_4\cdot(MeCN)_2\cdot(H_2O)_2\}_x$; Color code: blue – axle, red – DB24C8, dark blue – metal ion, yellow – MeCN, green – H_2O. (Figure from reference 34).

I.4. Our approach

Despite the advances in this field, the design and synthesis of metal-based interlocked architectures still remains a challenging issue in synthetic chemistry. This situation stems from the fact that, while several complementary recognition sites could be used in the template-based synthesis of a ‘‘rota-ligand”, not all of them are robust enough to withstand the ensuing coordination process, which often requires either strongly donating polar solvents that disrupt the non-covalent interactions holding the pseudorotaxane together, or elevated temperatures.

As mentioned above, pseudorotaxane and rotaxane structures consist of one or more macrocycles threaded by one or more axles, and their general nomenclature is *[n]rotaxane*, where the number inside the brackets indicates the total number of components in the assembly. This originates from the fact that all these species prepared to date are templated by recognition sites incorporated into axles having only *two side-arms* protruding from the cavity of the wheel. We wish to present here a new recognition motif for the template-directed formation of pseudorotaxanes based on an axle that allows the extension of *four side-arms* directly from the cavity of the crown ether, and thus positioning the wheel component in a straddled orientation onto the axle, thus generating starburst (pseudo)rotaxanes. To differentiate between these two topologies, we will use here the following notation: [2_2] and [2_4]pseudorotaxanes; the first integer in square brackets designates the number of the components of the assembly (as in the original nomenclature of these species) and the second, placed as a subscript, indicates the number of side-arms protruding from the center of the macrocyclic component. This notation is schematically represented in Figure I.10.

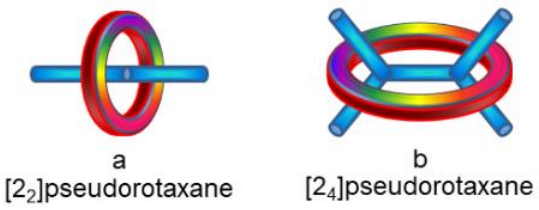

Figure I.12. Cartoon representations of: a) regular [2_2]pseudorotaxanes; and b) starburst [2_4]pseudorotaxanes. (Figure from reference 35).

In one of his seminal early papers,[27] Stoddart noted that, in contrast to all viologens, the $[BipyH_2]^{2+}$ dication (Scheme I.3.a) is completely encapsulated by BPP34C10, with the formation of two strong and nearly linear N^+-H···O hydrogen bonds with the central oxygen atoms on the polyether linkage and of strong aromatic π – π stacking interactions between the bipyridine and phenylene moieties.

Benzobis(imidazolium) salts ($[BBI\text{-}H_2\text{-}R_4]^{2+}$, R = alkyl, aryl, Scheme I.3.b) are shorter than $BipyH_2^{2+}$ and have two positive charges localized on the N-CH-N regions, thus making the C2 hydrogen atoms highly acidic. We reasoned that, in resemblance with the $BipyH_2^{2+}$ dication, these H atoms could be involved in H-bonding with the O atoms within the ethyleneglycol chains of the crown ethers. $[N\text{-}CH\text{-}N]^+ \cdots O$ ion-dipole interactions between the positively charged atoms of the BBI^{2+} component and the Lewis basic atoms of the crown ether could also make a significant contribution to the binding.[28] Further, the BBI^{2+} dication consists of an electron deficient rigid framework with a π-conjugated linker between the two imidazolium moieties and could interact through π – π stacking interactions with the electron rich aromatic rings of the hosts. These characteristics make the BBI^{2+} salts excellent candidates for the template-directed formation of interlocked molecules in conjunction with BPP34C10 and 15DN38C10 wheels. More importantly, and in sharp contrast to the 4,4'-bipyridine based (pseudo)rotaxanes (and all other "two side-arms" examples), this recognition motif is easily functionalized with four side-arms through the N-atoms of the BBI^{2+} core, thus allowing the formation of starburst $[2_4]$pseudorotaxane architectures.

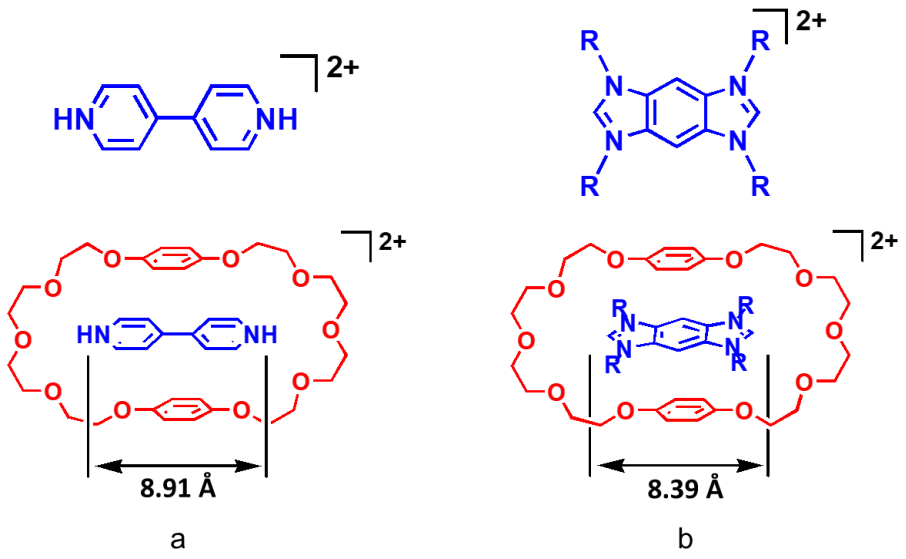

Scheme I.3. Comparison between a) $[BipyH_2]^{2+}$ and b) $[BBI\text{-}H_2\text{-}R_4]^{2+}$ dications and their interaction with BPP34C10. (Figure from reference 35).

I.5. References

1. Kim, M. *Chem. Soc. Rev*. **2002**, *31*, 96.

2. James, E. M.; Lewis, M. G.; Stephen, M. G. *Chem. Commun*, **2016**, 298.

3. Sauvage, J. P.; Amabilino, D. B. *Springer*. **2012**, *323*, 107.

4. Stoddart, J. F. *Chem. Soc. Rev*. **2009**, *38*, 1802.

5. Stoddart, J. F. *Angew. Chem. Int*. **2017**, *56*, 11094.

6. Liu, Y.; Vignon, S. A.; Zhang, X.; Bonvallet, P. A.; Khan, S. I.; Houk, K. N.; Stoddart, J. F. *J. Org. Chem*. **2005**, *70*, 9334.

7. Sauvage, J. P.; Buchecker, D. C. *Wiley-VCH*. **1999**, 1.

8. Forgan, S. R.; Sauvage, J. P.; Stoddart, J. F. *Chem. Rev*. **2011**, *111*, 5434.

9. Balzani, V.; Credi, A.; Raymo, F. M.; Stoddart, J. F., *Angew. Chem. Int.* **2000**, *39*, 3348.

10. Ashton, P. R.; Chrystal, E. J. T.; Menzer, S. G.; Schiavo. C.; Spencer, N.; Stoddart, J. F.; Tasker, P. A.; White, A. J. P.; Williams, D. J. *Chem. Eur. J*. **1996**, 709.

11. Coutrot, F.; Romuald, C.; Busseron, E.; *Org. Lett.* **2008**, *10*, 3741.

12. Loeb, S. J. *Chem. Soc. Rev*. **2007**, *36*, 226.

13. Martinez-Diaz, M. V.; Spencer, N.; Stoddart, J. F. *Angew. Chem. Int Ed*. **1997**, *36*, 1904.

14. Fernando, I. R.; Bairu, S. G.; Ramakrishna, G.; Mezei, G. *New J. Chem.* **2010**, *34*, 2097.

15. Pascu, S. I.; Naumann, C.; Kaiser, G.; Bond, A. D.; Sanders, J. K. M.; Jarrosson, T. *Dalton Trans*. **2007**, 3874.

16. Baum, R. R.; Veach, J. J.; Semeniuc, R. F.; Wheeler, K. A.; Pellechia, P. J. *Inorg. Chim. Acta*. **2017**, *455*, 52.

17. Balzani, V.; Credi, A.; Venturi, M. *Chem. Soc. Rev*. **2009**, *38*, 1542.

18. Green, J. E.; Choi, J. W.; Boukai, A.; Bunimovich, Y.; Johnston, H. E.; DeIonno, E.; Luo, Y.; Sheriff, B. A.; Xu, K.; Shin, Y. S.; Tseng, H. R.; Stoddart, J. F.; Heath, J. R. A. *Nat. Chem*. **2007**, *445*, 414.

19. Coskun, A.; Spruell, J. M.; Barin, G.; Dichtel, W. R.; Flood, A. H.; Botros, Y. Y.; Stoddart, J. F. *Chem. Soc. Rev*. **2012**, *41*, 4827.

20. Sean, W.; Robinson.; Beer,P.D. *Chem. Eur. J*. **2016**, 15, 153.

21. Langton, M. J.; Marques, I.; Robbinson, S. W.; Felix, V.; Beer, P. D.; *Chem. Eur. J*. **2017**, *22*, 185.

22. Li, Z.; Barnes, J. C.; Bosoy, A.; Stoddart, J. F.; Zink, J. I. *Chem. Soc. Rev*. **2012**, *41*, 2590.

23. Ambrogio, M. W.; Thomas, C. R.; Zhao, Y. L.; Zink, J. I.; Stoddart, J. F. *Chem. Res.* **2011**, *44*, 903.

24. Cotí, K. K.; Belowich, M. E.; Liong, M.; Ambrogio, M. W.; Lau, Y. A.; Khatib,H. A.; Zink, J. I.; Khashab, N. M.; Stoddart, J. F. *Chem. Soc. Rev*. **2009**, *1*, 16.

25. Ashton, P. R.; Fyfe, M. C. T.; Hickingbottom, S. K.; Menzer, S.; Stoddart, J. F.; White, A. J. P.; Williams, D. J. *Chem. Eur. J.* **1998**, *4*, 577.

26. Beer, P. D.; Vickers, M. S. *Chem. Soc. Rev*. **2007**, *36*, 211.

27. McGonigal, P. R. *Supramol Chem.* **2018**, *30*, 782.

28. Wu, J.; Leung, K. C. F.; Stoddart, J. F. *Proc. Natl. Acad. Sci*. **2007**, *104*, 17266.

29. Bo, G. D.; Dolphijn, G.; Mcternan, C. T.; Leigh, D. A. *J. Am. Chem. Soc*. **2017**, *139*, 8455.

30. James, J. E. M.; Beer, P. D.; Loeb, S. J.; Goldup, S. M. *Chem. Soc. Rev*. **2017**, *46*, 2577.

31. Loeb, S. J. *Chem. Commun.* **2005**, *12*, 1511.

32. Loeb, S. J.; Vukotic, V. N.; *Chem. Soc. Rev*. **2012**, *41*, 5896.

33. Whang, D.; Jeon, Y. M.; Heo, J.; Kim, K. *J. Am. Chem. Soc*. **1996**, *118*, 11333.

34. Davidson, G. J. E.; Loeb, S. J. *Angrew. Chem. Int. Ed*. **2003**, *42*, 74.

35. Foster, M. W.; Mehl, B. T.; Treadwell, E. M.; Semeniuc, R. F.; Wheeler, K. A. *Chem. Commun.* **2019**, *55*, 1786.

II. Experimental

II.1. General considerations

Unless otherwise noted, all operations were performed in ambient atmosphere. Experiments requiring oxygen and moisture free conditions were carried out under an inert gas (nitrogen or argon) atmosphere, using standard Schlenk techniques or a MBraun LabStar dry box. When needed, solvents were dried by conventional methods and distilled under a dry N_2 atmosphere immediately prior to use. NMR spectra were recorded using a 400 MHz Bruker Avance FT-NMR Spectrometer. 1,3-Dichloro-4,6-dinitrobenzene,[1] benzobis(imidazole),[2] and bis-1,5-(dinaphtho)-38-crown-10 (15DN38C10)[3,4,5] were prepared as described in the literature. For convenience, the synthetic steps are described below. All other reagents were commercially available (Sigma-Aldrich, Acros, TCI America, Oakwood) and used without further purification.

II.2. Synthesis of the axle components

The synthesis of the two-arm axle is depicted in Scheme II.1.

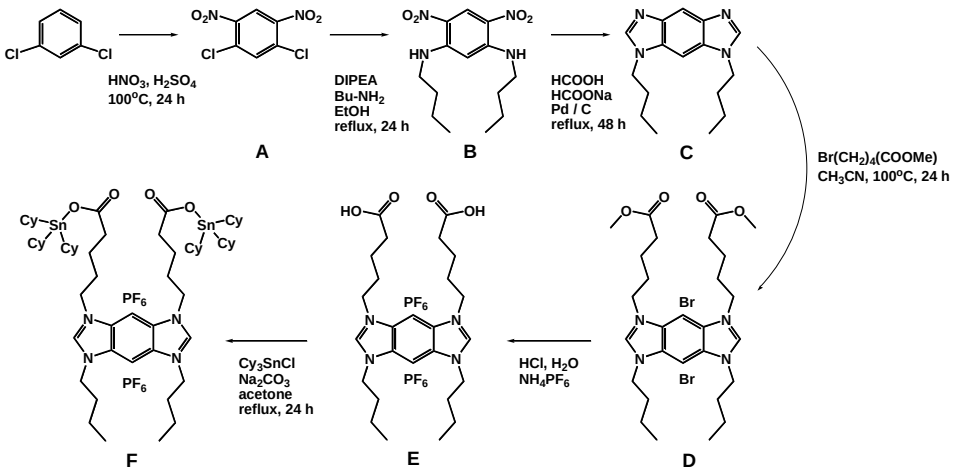

Scheme II.1. Reaction pathway for the preparation of the two-arm axle.

II.2.1. Synthesis of $C_6H_2Cl_2(NO_2)_2$, intermediate A. 1,3-Dichlorobenzene (15 mL, 132 mmol) was added dropwise to a solution of fuming HNO_3 (150 mL) and concentrated H_2SO_4 (80 mL) at 0 ˚C. The mixture was heated at 100 ˚C for 24 h and then poured into ice-cold water and extracted with ethyl acetate. The combined extracts were washed with water, saturated aqueous $NaHCO_3$ and brine. The organic layer was dried over $MgSO_4$, filtered and concentrated *in vacuo*. The residue was redissolved in ethyl acetate, and then n-hexane was added to the residue until a precipitate formed. This precipitate was collected by filtration, to give the product as a light-yellow solid (29.5 g, 94.7 %). ^{1}H-NMR (400 MHz, $CDCl_3$) δ: 8.57 (s, 1H), 7.83 (s, 1H). This ^{1}H-NMR spectrum is identical with the one previously reported in the literature.[1]

II.2.2. Synthesis of $C_6H_2(NO_2)_2(NHBu)_2$, intermediate B. Compound **A** (2.370 g, 10 mmol) was added to a round bottom flask (100 mL). Ethanol (30 mL), excess N,N-diisopropylethylamine (10.5 mL, 60 mmol) and 1-aminobutane (1.463 g, 20 mmol) were also added to the flask. The mixture was refluxed for 36 hours. After that, it was cooled down to room temperature and filtered to collect the product (2.969 g, 95.7%) as a yellow powder. ^{1}H-NMR (400 MHz, $CDCl_3$) δ: 9.23 (s, 1H), 8.31 (s, 2H), 5.65 (s, 1H), 3.30-3.26 (q, 4H), 1.79-1.72 (quintet, 4H), 1.55-1.46 (sextet, 4H), 1.03-0.09 (t, 6H).

II.2.3. Synthesis of $BBI(Bu)_2$, intermediate C. Compound **B** (2.969 g, 9.6 mmol) was reacted with formic acid (100 mL), sodium formate (115 g, 1691 mmol) and Pd/C (10%, 1.0 g) in a round bottom flask. The mixture was refluxed under nitrogen for 48 hours. The mixture was cooled down to room temperature and filtered through celite with the aid of

water (50 mL). The volume of the filtrate was reduced approximately to 50 mL under reduced pressure. Then, it was added to a vigorously stirred solution of saturated potassium carbonate. The light brown precipitated solid was collected by filtration. (2.197 g, 84.9 %). ^{1}H-NMR (400 MHz, $CDCl_3$) δ: 8.19 (s, 1H) , 7.92 (s, 2H), 7.21 (s, 1H), 4.23-4.20 (t, 4H), 1.96-1.87 (quintet, 4H), 1.45-1.36 (sextet, 4H), 1.00-0.96 (t, 6H).

II.2.4. Synthesis of {BBI(Bu)$_2$[(CH$_2$)$_4$COOMe]$_2$}Br$_2$, intermediate D. Compound **C** (2.0 g, 7.4 mmol) and acetonitrile (30 mL) were mixed with ethyl 5-bromovalerate (3.463 g, 17.8 mmol) in a high pressure tube. The reaction was carried out overnight at 100 °C. The reaction mixture was cooled down to room temperature and the solvent removed under reduced pressure to isolate the product as a white powder (3.119 g, 63.8%). ^{1}H-NMR (400 MHz, DMSO-d_6) δ:10.01 (s, 1H), 9.05(s, 2H), 4.88-4.81 (q, 8H), 3.61 (s, 6H), 2.28-2.13 (quintet, 8H), 1.82-1.74 (t, 4H), 1.57-1.47 (t, 4H), 1.01-0.97 (t, 6H).

II.2.5. Synthesis of {BBI(Bu)$_2$[(CH$_2$)$_4$COOMe]$_2$}(PF$_6$)$_2$, intermediate E. Compound **D** (1.010 g, 1.5 mmol) was heated overnight in a solution made of concentrated hydrochloric acid (1 mL) and deionized water (50 mL). After the mixture was cooled down to room temperature, excess ammonium hexafluorophosphate (0.815 g, 5.0 mmol) was added to the solution. The precipitated product was isolated by vacuum filtration as a white powder (1.096 g, 93.9 %). ^{1}H-NMR (400 MHz, acetone-d_6) δ: 10.02 (s, 2H), 9.06 (s, 1H), 4.88-4.81 (m, 8H), 2.44-2.40 (t, 4H), 2.29-2.13 (m, 9H), 1.82-1.57 (t, 4H), 1.01-0.97 (t, 6H).

II.2.6. Synthesis of the $\{BBI(Bu)_2[(CH_2)_4COOSnCy_3]_2\}(PF_6)_2$ axle, F. A round bottom flask was charged with a magnetic stir bar and compound **E** (0.0762 g, 0.1 mmol). Acetone (40 mL), tricyclohexyltin chloride (0.0807 g, 0.2 mmol) and sodium carbonate (0.0106 g, 0.1 mmol) were added, and the mixture was refluxed for 24 hours. After cooling to room temperature, the solution was filtered to remove the inorganic materials, then the solvent was evaporated to obtain the desired product as a white powder (0.0886 g, 59.2 %). ^{1}H-NMR (400 MHz, acetone) δ: 10.08 (s, 2H), 9.11 (s, 1H), 4.89-4.82 (m, 9H), 2.44-2.41 (t, 4H), 2.29-2.13 (m, 10H)1.16-1.57 (m, 68H),1.01-0.97(t, 4H).

The synthesis of the four-arm axle is depicted in Scheme II.2.

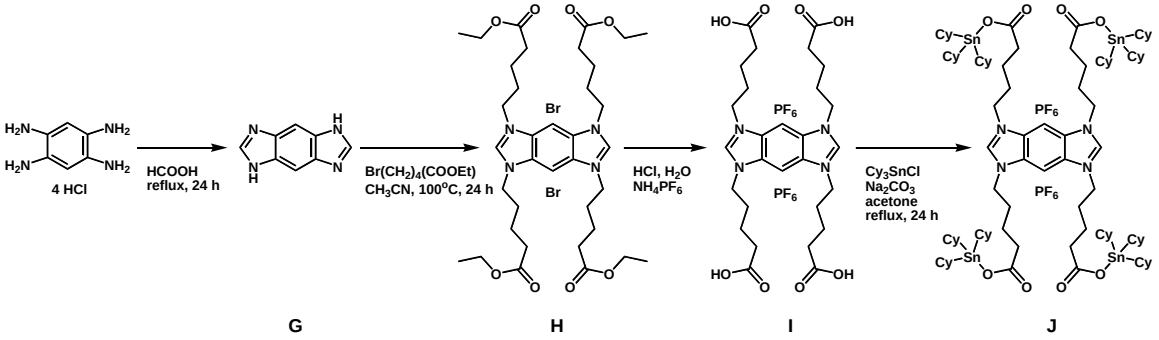

Scheme II.2. Reaction pathway for the preparation of the four-arm axle.

II.2.7. Synthesis of benzobis(imidazole), intermediate G. A magnetic stir bar, 1,2,4,5-benzenetetraamine tetrahydrochloride (2.84 g, 10 mmol), and formic acid (88-99%, 75 mL) were added to a round bottom flask. The mixture was heated and refluxed overnight. Then, the condenser was replaced with a distillation head and the volume of the solution was reduced to approximately 10 mL. The remaining solution was removed under vacuum. Then the obtained solid was dissolved in water and filtered to remove any solid impurities.

The pH of the filtrate was adjusted to 6.5-6.8 with 10% NaOH. The precipitate was collected by vacuum filtration. It was rinsed with cold water and dried under vacuum over P_2O_5 to afford desired compound (1.36 g, 85.9 %) as a light brown solid. ^{1}H-NMR (400 MHz, DMSO-d_6): δ 8.18 (s, 2H, C2-H), 7.69 (s, 2H, C_6H_2).

II.2.8. Synthesis of {BBI[$(CH_2)_4COOH]_4$}$(PF_6)_2$, intermediate I. Ethyl-5-bromovalerate (3.377 g, 15 mmol), sodium carbonate (1.059 g, 10 mmol) and compound G (0.395 g, 2.5 mmol) were reacted in a high-pressure tube charged with a magnetic stir bar, using acetonitrile (50 mL) as the solvent. The reaction was carried out for 48 hours at 95 °C. The reaction mixture was cooled down to room temperature, then the volatiles were removed under reduced pressure, to obtain the crude product as a white powder. Without isolation and any characterization, intermediate H was heated overnight in concentrated hydrochloric acid (1 mL) and deionized water (50 mL). The mixture was then cooled down to room temperature and ammonium hexafluorophosphate (1.63 g, 10 mmol) was added to the solution. The crude product was isolated by vacuum filtration. The pure compound was isolated after several recrystallizations from an acetone / ethanol / diethyl ether solvent mixture (1:0.5:10); this procedure afforded 0.251 g (11.8 %) of the desired product as a white powder. ^{1}H-NMR (400 MHz, acetone-d_6) δ: 10.09 (s, 2H), 9.09 (s, 2H), 4.89-4.86 (t, 8H), 2.44-2.40 (quintet, 8H), 2.30-2.22 (quintet, 8H), 1.82-1.74 (t, 8H).

II.2.10. Synthesis of the {BBI[$(CH_2)_4COOSnCy_3]_4$}$(PF_6)_2$ axle, J. A round bottom flask was charged with a magnetic stir bar and compound **I** (0.0851 g, 0.1 mmol). Acetone (40 mL), tricyclohexyltin chloride (0.1614 g, 0.4 mmol) and sodium carbonate (0.0212 g, 0.02

mmol) were added, and the mixture was refluxed for 24 hours. After cooling to room temperature, the solution was filtered to remove the inorganic materials, then the solvent was evaporated to obtain the desired product as a white powder (0.1364 g, 58.8%). ^{1}H-NMR (400 MHz, acetone) δ: 10.08 (s, 2H), 9.11 (s, 1H), 4.89-4.82 (m, 9H), 2.44-2.41 (t, 4H), 2.29-2.13 (m, 10H) 1.16-1.57 (m, 68H),1.01-0.97 (t, 4H).

II.3. Synthesis of the bis-1,5-(dinaphtho)-38-crown-10 (15DN38C10) wheel

The synthesis of the 15DN38C10 wheel is depicted in Scheme II.3.

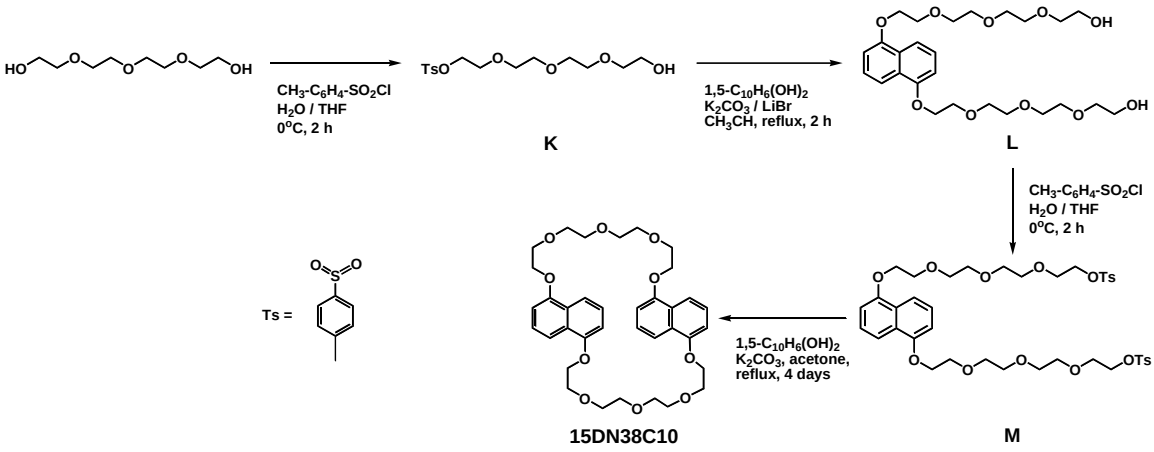

Scheme II.3. Reaction pathway for the preparation of the 15DN38C10 crown ether.

II.3.1. Synthesis of CH_3-C_6H_4-(CH_2-CH_2-O)$_4$H, intermediate K. A solution of NaOH (2.74 g, 68.5 mmol) in water (15 mL) was added to a mixture of tetraethylene glycol (87.8 g, 452 mmol) and THF (15 mL). After mixture had cooled down to 0 °C, a solution of p-toluenesulfonyl chloride (8.7 g, 45.6 mmol) in THF (50 mL) was added while stirring for 1 h. After stirring at 0 °C for 2 h, the reaction mixture was poured into ice water (250 mL). The organic layer was separated. The aqueous layer was extracted with CH_2Cl_2 (3x100

mL). The combined organic layers were dried over $MgSO_4$ and evaporated under reduced pressure, to afford the desired compound as a colorless oil (12.9 g, 81.2 %). ^{1}H-NMR (400 MHz, $CDCl_3$) δ: 7.86-7.76 (d, 2H), 7.35-7.31 (d, 2H), 4.17-4.12 (m, 2H), 3.70-3.58 (m, 14H), 2.43 (s, 3H).

II.3.2. Synthesis of $C_{10}H_6[(O\text{-}CH_2\text{-}CH_2)_4\text{-}OH]_2$, intermediate L. 1,5-Dihydroxy-naphthalene (5.23 g, 32.7 mmol) was added to a mixture of tetraethyleneglycol monotosylate (K) (22.75 g, 65.3 mmol), K_2CO_3 (17.85 g, 129.2 mmol), and a catalytic amount of LiBr (1.5 g) in MeCN (250 mL).The reaction mixture was heated under reflux for 24 h and was filtered after cooling. The residue was dissolved in water (200 mL), and the resulting solution was extracted with CH_2Cl_2 (2x50 mL). The organic layer was combined with previously obtained filtrate and evaporated in vacuo. The resulting brown oil was dissolved in CH_2Cl_2 (200 mL), and the solution was washed carefully with a mixture of brine and 10% aq. NaOH (3:1, 3 x 100 mL). The organic layer was dried over $MgSO_4$, and the solvent was removed under vacuo to afford the title compound as a light-brown oil (8.36 g, 50%). ^{1}H-NMR (400 MHz, $CDCl_3$) δ: 7.86 (d, 2H), 7.35 (t, 2H), 6.84 (d, 2H), 4.30 (t, 4H), 4.01 (t, 4H), 3.56-3.87 (m, 24H), 2.51 (t, 2H).

II.3.3. Synthesis of $C_{10}H_6[(O\text{-}CH_2\text{-}CH_2)_4\text{-}O\text{-}C_6H_4\text{-}CH_3]_2$, intermediate M. Intermediate L (4.377 g, 8.54 mmol) was dissolved in THF (12 mL). A solution of NaOH (1.5 g, 37.5 mmol) in water (7.0 mL) was added to the mixture. This mixture was cooled in an ice bath to 0 $^{\circ}$C. A solution of p-toluenesulfonyl chloride (3.35 g, 17.6 mmol) in THF (30 mL) was added while stirring the medium for over 2 h. The internal temperature was kept below 5

°C. After the addition was completed, stirring was continued at room temperature for 2 h. The reaction mixture was poured into ice water (70 mL) and was extracted with 3x100 mL CH_2Cl_2. The combined organic layers were dried over $MgSO_4$ and the solvent was removed under vacuo (3.981 g, 56.8 %). ^{1}H-NMR (400 MHz, $CDCl_3$) δ: 7.86 (d, 2H, J = 8.52 Hz), 7.77 (d, 4H, J = 8.2 Hz), 7.35-7.28 (m, 6 H), 6.84 (d, 2H, J = 7.64 Hz), 4.28 (t, 4H, J = 4.68 Hz), 4.12 (t, 4H, J = 4.76 Hz), 3.98 (t, 4H, J = 4.88 Hz), 3.79-3.72 (m, 16H), 3.60-3.55 (m, 4H), 2.41 (s, 6H).

II.3.4. Synthesis of the 15DN38C10 crown ether. 1,5-Dihydroxynaphthalene (0.16 g, 1.0 mmol) and intermediate M (0.82 g, 1.0 mmol) were dissolved in acetone (40 mL) and were injected into a suspension of K_2CO_3 (7 g, 51 mmol) in acetone (200 mL) at a rate of 0.8 mL/h under reflux and the reaction was allowed to proceed for 70 h. The reaction mixture was cooled down to room temperature, filtered. The filtrate was washed with $CHCl_3$ (50 mL). The solvent evaporated from the filtrate and the residue was partitioned between H_2O (100 mL) and $CHCl_3$.The organic layer was extracted with $CHCl_3$ (2x75 mL). These organic extracts were combined, and the solvent was evaporated to afford a brown oil (100 mg, 16%). ^{1}H-NMR (400 MHz, $CDCl_3$) δ: 7.79 (d, 4H), 7.19 (t, 4H), 6.50 (d, 4H), 4.06 (m, 8H), 3.93 (m, 8H), 3.78 (m, 8H), 3.75 (m, 8H). This ^{1}H-NMR spectrum is identical with the one previously reported in the literature.[5]

II.4. NMR titrations

^{1}H-NMR titrations were conducted in acetone-d_6 at 293 K. To 500 μL of a 5.12 x 10^{-4} M solution of the crown were added aliquots of the axles. Titration points for 0, 0.1, 0.2, 0.3,

0.4, 0.5, 0.6, 0.7, 0.8, 0.9, 1.0, 1.1, 1.2, 1.3, 1.4, 1.5, 1.6, 1.7, 1.8, 1.9, 2.0, 2.5, and 3.0 equivalents of axles were obtained in each case. The sample was thoroughly shaken before taking the ^{1}H NMR spectrum. The chemical shift of the protons situated on the aromatic region of the crown was monitored. The average of three independent measurements was used for the determination of the association constant K_a using the Bindfit online software.[6.7]

II.5. Crystallography

{BBI[$(CH_2)_4COOH$)]$_4$}$(PF_6)_2$ and a slight excess of 15DN38C10 were dissolved in the minimum amount of acetone (*ca*. 20 mL). Chloroform (about 1 mL) was added to the solution to enhance the solubility of the crown. The resulting cloudy solution was filtered through a plug of cotton wool. The filtrate was equally divided into four separate 1-dram vials. Each of the vials were inserted into four 5-dram vials, having diethyl ether up to about half of their volume. All vials were capped and kept undisturbed for a few days until the crystals appeared on the wall of the inside vials.

A specimen of $C_{65}H_{86}F_{12}N_4O_{20}P_2$, approximate dimensions 0.130 mm x 0.160 mm x 0.190 mm, was used for the X-ray crystallographic analysis. The X-ray intensity data were measured (λ = 1.54178 Å). A total of 6528 frames were collected. The total exposure time was 18.13 hours. The frames were integrated with the Bruker SAINT software package using a narrow-frame algorithm. The integration of the data using a triclinic unit cell yielded a total of 21595 reflections to a maximum θ angle of 61.30° (0.88 Å resolution), of which 5310 were independent (average redundancy 4.067, completeness = 96.9%, R_{int} =

6.57%, R_{sig} = 4.77%) and 3879 (73.05%) were greater than $2\sigma(F^2)$. The final cell constants of a = 10.6162(3) Å, b = 13.1131(3) Å, c = 13.3143(3) Å, α = 102.510(2)°, β = 94.844(2)°, γ = 98.423(2)°, volume = 1776.98(8) $Å^3$, are based upon the refinement of the XYZ-centroids of 119 reflections above 20 σ(I) with 6.944° < 2θ < 90.48°. Data were corrected for absorption effects using the Multi-Scan method (SADABS). The ratio of minimum to maximum apparent transmission was 0.882. The calculated minimum and maximum transmission coefficients (based on crystal size) are 0.7650 and 0.8300. The structure was solved and refined using the Bruker SHELXTL Software Package, using the space group P-1, with Z = 1 for the formula unit, $C_{65}H_{86}F_{12}N_4O_{20}P_2$. The final anisotropic full-matrix least-squares refinement on F^2 with 482 variables converged at R1 = 4.90%, for the observed data and wR2 = 13.35% for all data. The goodness-of-fit was 1.040. The largest peak in the final difference electron density synthesis was 0.483 $e^-/Å^3$ and the largest hole was -0.256 $e^-/Å^3$ with an RMS deviation of 0.057 $e^-/Å^3$. On the basis of the final model, the calculated density was 1.433 g/cm^3 and F(000), 802 e^-. [8-11]

II.6. References

1. Takayama, Y.; Yamada, T.; Tatekabe, S.; Nagasawa, K. *Chem. Comm*. **2013**, *49*, 6519.

2. Boydson, A. J.; Pecinovsky, C.S.; Chao, S.T.; Bielawski, C.W. *J. Am. Chem. Soc*. **2007**, *129*, 14550.

3. Shirude, P. S.; Kumar, V. A.; Ganesh, K. N. *Eur. J. Org, Chem*. **2005**, 5207.

4. Ashton, P. R.; Huff, J.; Menzer, S.; Parsons, I. W.; Preece, J. A.; Stoddart, J. F.; Tolley, M. S.; White, A. J. P.; Williams, D. J. *Eur. J. Chem*. **1996**, *2*, 40.

5. Bruns, C. J.; Basu, S.; Stoddart, J. F. *Tetrahedron Lett.* **2010**, *51*, 983.

6. Bindfit: http://supramolecular.org

7. Hibbert, B. D.; Thordarson, P. *Chem. Commun.* **2016**, *52*, 12792.

8. **SAINT+** Version 8.37A. Bruker AXS, Inc., Madison, Wisconsin, USA, 2016.

9. **SADABS**-2016/2: Krause, L.; Herbst-Irmer, R.; Sheldrick G. M.; Stalke D. *J. Appl. Cryst.* **2015**, *48*, 3.

10. **SHELXT**: Sheldrick, G. M. *Acta Cryst*. **2015**, *A71*, 3.

11. **SHELXL:** Sheldrick, G. M. *Acta Cryst*. **2015**, *C71*, 3.

III. Results and Discussion

Since Pedersen published in 1967 his seminal paper on the cation complexation by a series of crown ethers,[1] these species and their derivatives have become key components in the chemistry of the mechanical bond.[2-8] The threading of viologen species through the cavities of crown ethers such as bis(para-phenylene)-34-crown-10 (BPP34C10) and bis-1,5-(dinaphtho)-38-crown-10 (15DN38C10) to form $[(\text{viologen})\subset(\text{crown ether})]^{2+}$ interlocked architectures lies at the foundation of a wide range of pseudorotaxane and rotaxane systems. As mentioned before, benzobis(imidazolium) salts (BBI) have several characteristics that would make these species good candidates for the synthesis of interlocked species in combination with crown ethers, thus generating $[2_4]$pseudorotaxane architectures.[9] The following describes the synthesis and characterization of two benzobis-(imidazolium) axles with donor capabilities, their complexation with metallic centers, and the investigations related to their interaction with the 15DN38C10 crown ether.

III.1. Synthetic Considerations

Two axle components were synthesized: one (a ditopic axle) having two carboxylic groups, and another (tetratopic) with four such donor groups attached to the central BBI core. The synthesis of the ditopic axle (see Scheme III.1) started with the reaction of *n*-dichloro-benzene with H_2SO_4, HNO_3 at 0°C by refluxing in 100°C for 24 hours. The reaction added two nitro groups to the 1,3-dichlorobenzene and thus forming 1,3-dichloro-4,6-dinitro-benzene. After replacing the two Cl atoms with aminobutane groups, it was then converted

into the 1,3-dibutylbenzobisimidazole derivative **C**, via a reduction / ring closing reaction. Addition of the ester side-arms followed, by the reaction between **C** and methyl 5-bromo-pentanoate in acetonitrile. The hydrolysis of the ester group was achieved by using HCl and distilled water to obtain the carboxylic acid. The Br^- / PF_6^- anion exchange was achieved with ammonium hexafluorophosphate. The final step was to attach the tricyclohexyltin center (Cy_3Sn) to the axle, by the reaction of the carboxylic species with tricyclohexyltin chloride in the presence of sodium carbonate, using acetone as a medium.

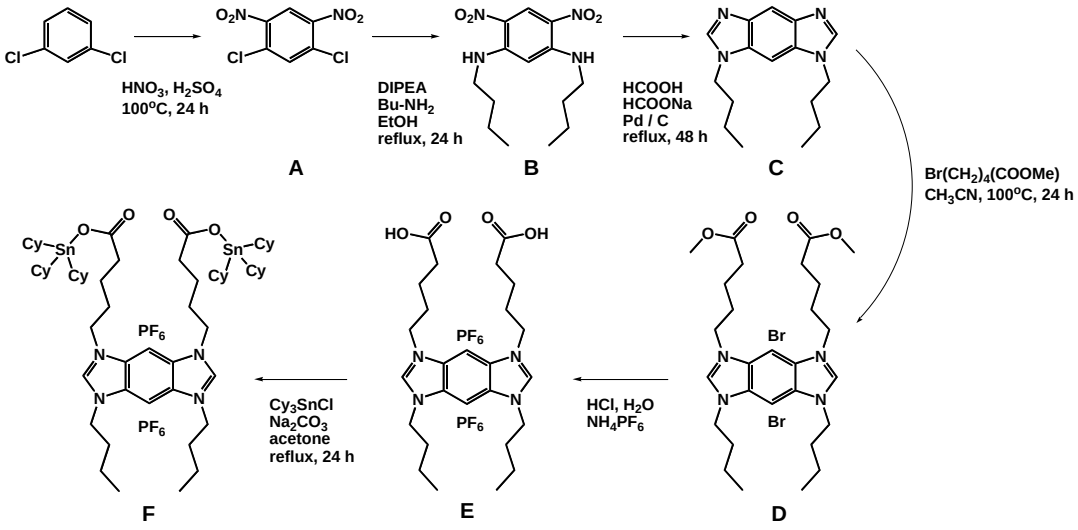

Scheme III.1. Reaction steps taken for the preparation of the two-arm axle.

The synthesis of the tetratopic axle is depicted in Scheme III.2 and started with the synthesis of the BBI from 1,2,4,5-benzenetetraamine tetrahydrochloride and formic acid. To introduce the four identical arms, ethyl 5-bromovalerate was reacted with BBI in acetonitrile as the solvent. Hydrolysis, anion exchange and metal complex introduction were done using the same reactions which were used in the synthesis of the two-arms axle described above.

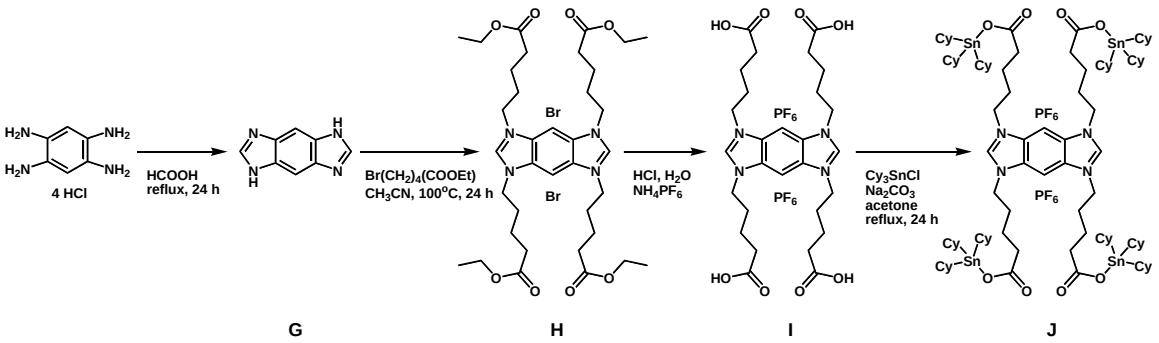

Scheme III.2. Reaction steps taken for the preparation of the four-arm axle.

The crown ether 15DN38C10 was synthesized starting with the monotosylation of tetraethylene glycol. The tosylated tetraethylene glycol was then reacted with 1,5-bishydroxynaphthalene to obtain the 1,5-bis[2-[2-(2-hydroxyethoxy)ethoxy]ethoxy]-naphthalene. The hydroxyl groups were tosylated again and the product was then reacted with 1,5-bis-hydroxynaphthalene, to afford the desired compound. The synthetic steps are shown in Scheme III.3.

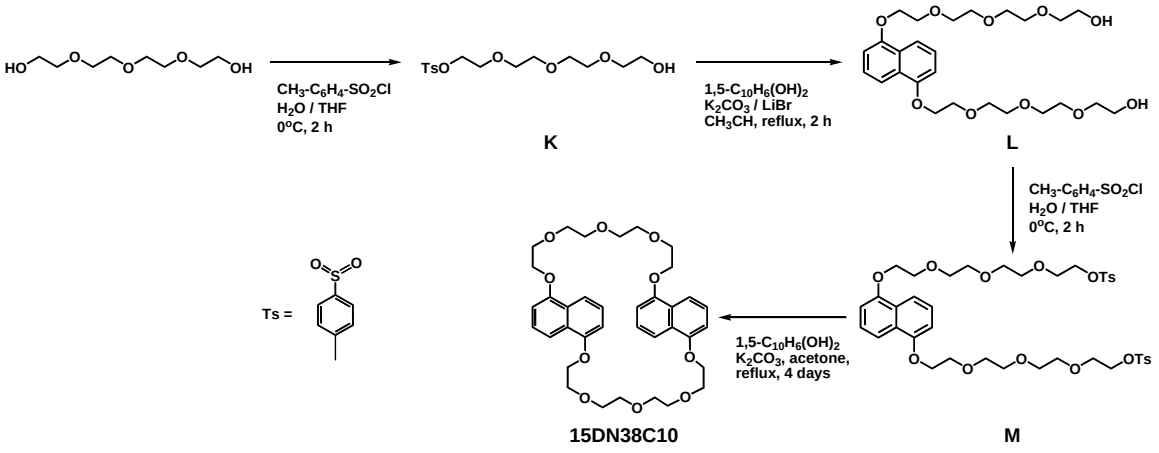

Scheme III.3. Reaction steps taken for the preparation of the 15DNC10 crown ether.

III.2. Spectroscopic Characterization

All intermediates and final compounds were characterized by NMR spectroscopy. The following describes the characterization of some important intermediates, as well as of the final axles.

III.2.1. Axles characterization

Two axles were prepared: the ditopic BBI-$(Bu)_2$-$[(CH_2)_4$-COO-$SnCy_3]_2$ (**F**, see Scheme III.1) and the tetratopic BBI-$[(CH_2)_4$-COO-$SnCy_3]_4(PF_6)_2$ (**J**, see Scheme III.2). In the synthesis of the axle **F** an important intermediate is dibutyl-benzobis(imidazole), BBI-$(Bu)_2$ (**C**). The ^{1}H-NMR of this compound (Figure III.1) shows the aromatic peaks around 8.1, 7.9 and 7.2 ppm in the expected 1 : 2 : 1 ratio, while the aliphatic protons are positioned around 4.2, 1.9, 1.4, and 0.9 ppm, respectively, with a 4 : 4 : 4 : 6 ratio. The "rota-ligand" BBI-$(Bu)_2$-$[(CH_2)_4$-$COOH]_2$ (**E**, Figure III.2) has the aromatic singlet signals at 10.0 and 9.0 ppm, and the aliphatic signals as multiplets 4.8 ppm and in the 2.4 – 0.97 ppm interval. The NMR of the final compound, BBI-$(Bu)_2$-$[(CH_2)_4$-COO-$SnCy_3]_2$ (**F**, Figure III.3) does not significantly differ from the parent ligand, the only difference consisting in the presence of additional peaks corresponding to the cyclohexyl groups onto the tin center in the aliphatic region of the spectrum. The ^{1}H-NMR of the tetratopic axle BBI-$[(CH_2)_4$-$COOH]_4(PF_6)_2$ (**I**) is presented in Figure III.4 and shows the aromatic protons at 10.0 ppm and 9.0 ppm, with the aliphatic groups in the 4.9 ppm – 1.7 ppm interval. Finally, the tetra-tin derivative BBI-$[(CH_2)_4$-COO-$SnCy_3]_4(PF_6)_2$ (**J**) shows the signal for the C2-H proton at 10.1 ppm while the hydrogen on the benzene ring appears at 9.1 ppm, see Figure III.5.

In addition, the aliphatic hydrogen atoms produced signals in the 4.9 ppm – 1.3 ppm interval, similar to the parent ligand **I**.

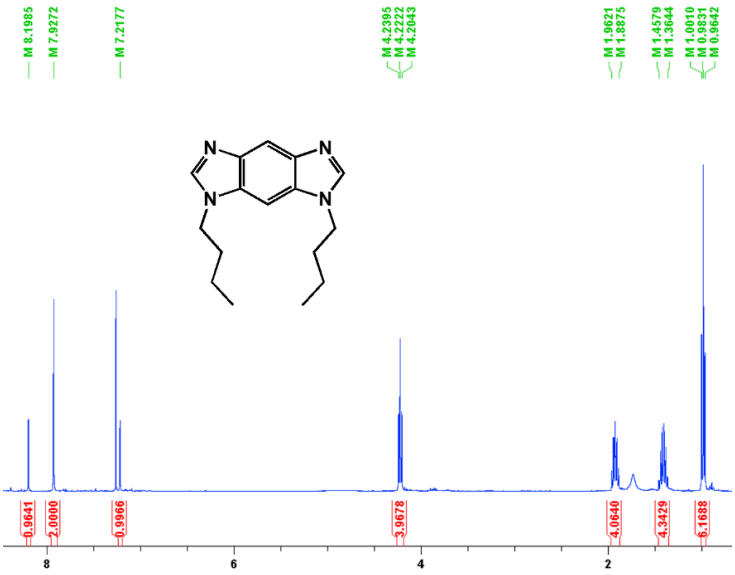

Figure III.1. Partial ^{1}H-NMR spectrum of intermediate **C**, BBI-$(Bu)_2$.

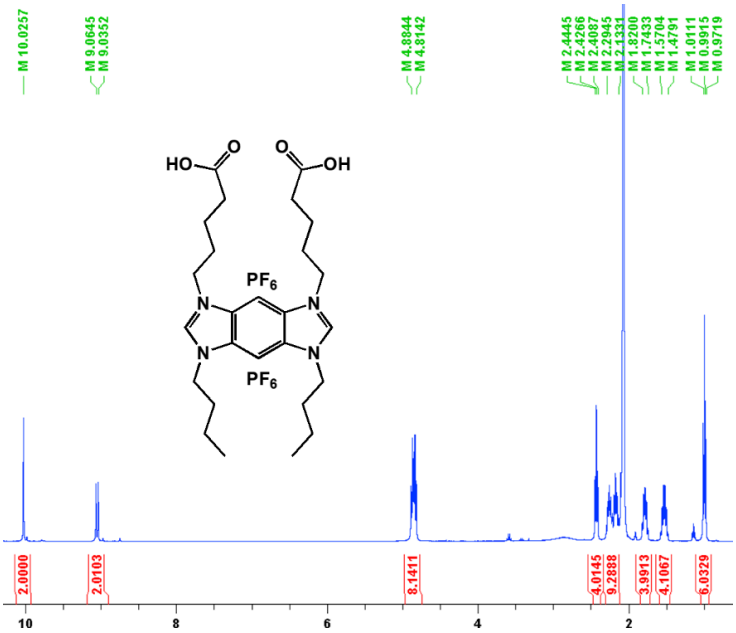

Figure III.2. Partial ^{1}H-NMR spectrum of intermediate **E**, BBI-$(Bu)_2$-$[(CH_2)_4$-$COOH]_2(PF_6)_2$

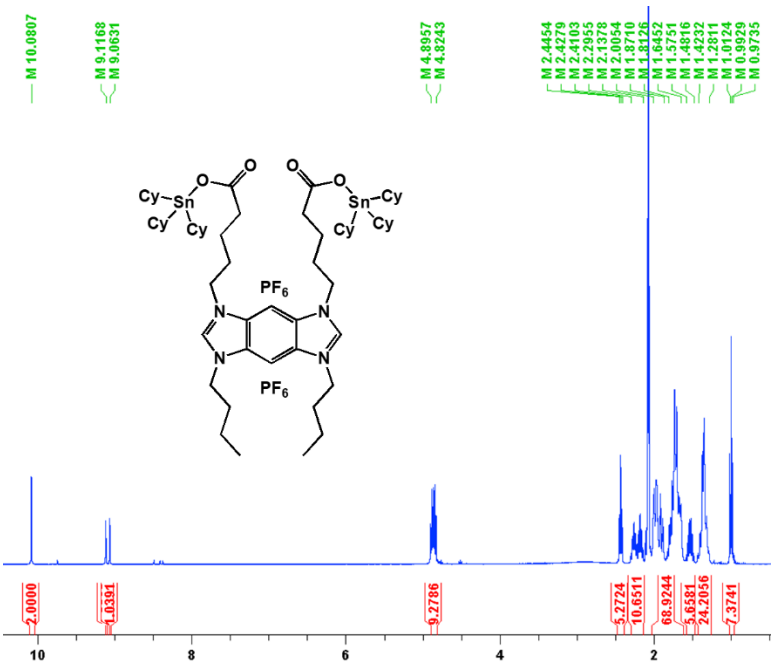

Figure III.3. Partial ^{1}H-NMR spectrum of the ditopic tricyclohexyltin-based axle **F**.

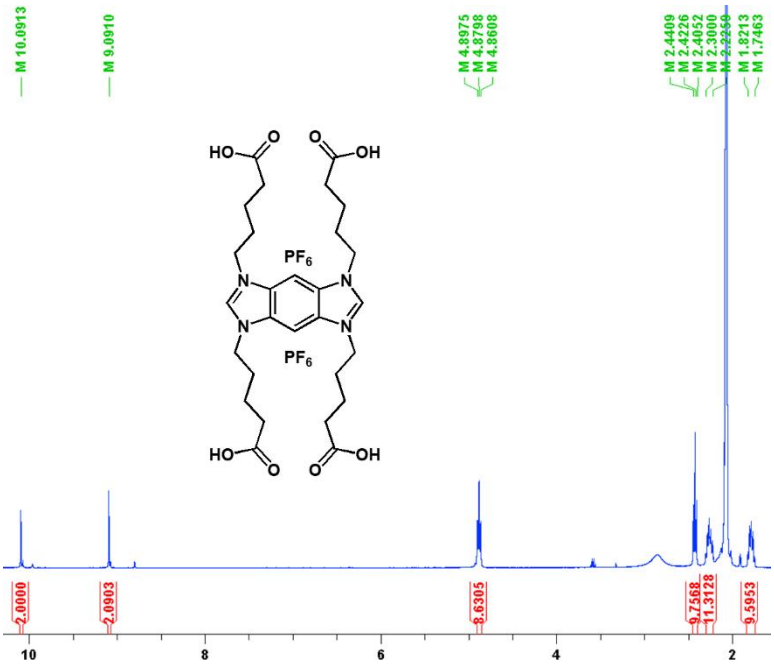

Figure III.4. Partial ^{1}H-NMR spectrum of intermediate **I**, BBI-[$(CH_2)_4$-COOH]$_4$(PF_6)$_2$.

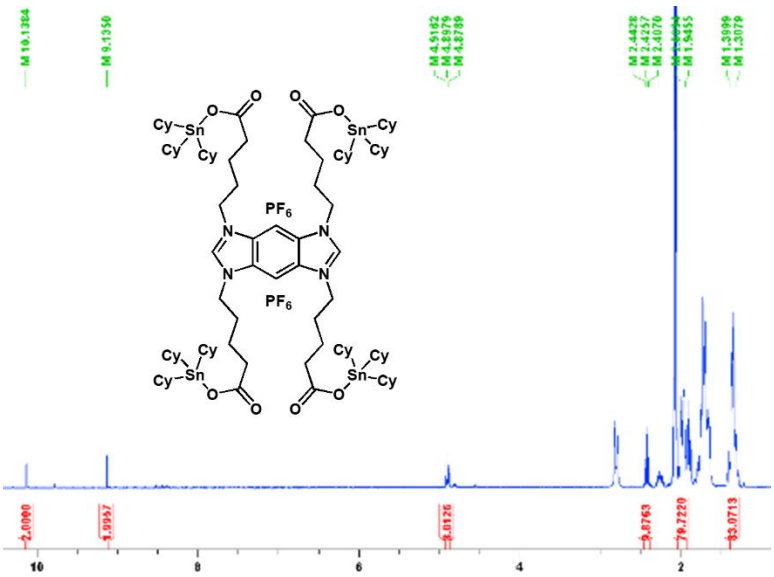

Figure III.5. Partial ^{1}H-NMR spectrum of the tetratopic tricyclohexyltin-based axle **J**.

III.2.2. Pseudorotaxane characterization.

Upon mixing equimolar solutions of the axles and crown ethers, two types of interactions can take place: the components can show a slow or a fast exchange on the NMR time scale. In the first instance, the slow rate of association and dissociation of the components on the NMR timescale permits the observation of three different sets of peaks in their NMR spectra, corresponding to the free axles and crown ether, and the [2]pseudorotaxane species. In the case of a fast exchange, only one signal for a specific proton is observed, an average between the uncomplexed and complexed chemical shift of the corresponding protons.

The pseudorotaxane systems presented here they all show a fast exchange on the NMR time scale, as it is exemplified in Figure III.6 with the BBI(Bu)$_2$[(CH$_2$)$_4$-COOH]$_2$

and15DN38C10 components. The Figure shows the changes in the NMR spectrum of the BBI(Bu)$_2$[(CH$_2$)$_4$-COOH]$_2$⊂15DN38C10 pseudorotaxane (the blue line at the bottom) after mixing equimolar solutions of the species, i.e. BBI(Bu)$_2$[(CH$_2$)$_4$-COOH]$_2$ axle (the green line at the top) and 15DN38C10 (the red line in the middle). All other examples investigated in this work presented a similar behavior to the one just described here.

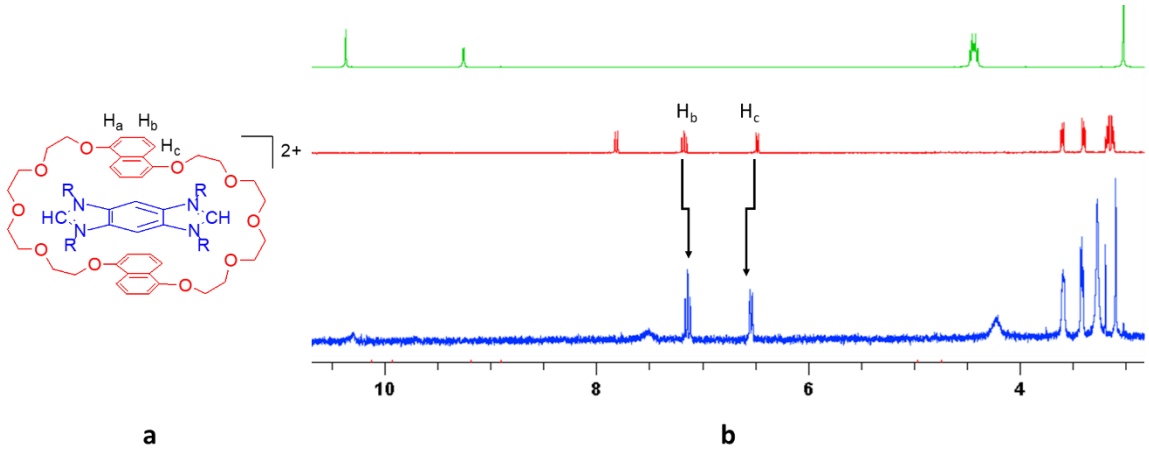

Figure III.6. a) Schematic view of the pseudorotaxanes studied in this work; b) changes in the NMR spectrum after the formation of the BBI(Bu)$_2$[(CH$_2$)$_4$-COOH]$_2$⊂15DN38C10 (blue line – bottom) from 15DN38C10 (red line – middle) and BBI(Bu)$_2$[(CH$_2$)$_4$-COOH]$_2$ (green line – top); color code: green – axle, red – crown, blue – pseudorotaxane.

III.3. Thermodynamic characterization

The next important aspect we focused on was to determine the association constant (K_a) of the pseudorotaxanes we synthesized. We have focused our attention on the interactions between axles **E** and **F**, as well as **I** and **J**, with the 15DN38C10 crown ether.

When it comes to finding the association constant of pseudorotaxanes, several methods can be used, depending on what type of process is taking place. In the case of a slow exchange on the NMR time scale, the single point method is used, where only one NMR spectrum is needed. If the system shows a fast exchange on the NMR time scale, only one signal for a specific proton is observed, making the determination of the K_a difficult. However, several methods are available, like the dilution or the titration method.

The formula to calculate the K_a starts from the equilibrium between the axle (**A**), the crown (**C**), and the pseudorotaxane (**R**), see equation (1). The second equation (2) shows the relationship between the equilibrium concentrations of the axle and crown and pseudorotaxane, expressed using the initial concentrations of the axle c(**A**) and crown c(**C**).

$$A + C \underset{}{\overset{K_a}{\rightleftharpoons}} R \quad (1)$$

$$K_a = \frac{[R]}{[A] \times [C]} = \frac{[R]}{\{(c(A) - [R]) \times (c(C) - [R]\}} \quad (2)$$

Since our system is fast on the NMR time scale (Figure III.6), to find the association constant for our pseudorotaxanes we used the titration method, where the concentration of one component is kept constant (in our case the crown), while the concentration of the other (the axle) is varied. The following expression (equation 3) can be derived,[10] and if

$\Delta\delta$ is measured, then the association constant K_a can be determined by non-linear curve-fitting.

$$\Delta\delta = \frac{\Delta\delta(\text{sat})}{c(A)} \times \frac{K_a\left(c(A)+c(C)\right)+1-\sqrt{[K_a\left(c(A)+c(C)\right)+1]^2-4\,{K_a}^2\times c(A)\times c(C)}}{2\,K_a} \quad (3)$$

Looking first at the interaction between axles **E** and **F** with 15DN38C10, we want to point out that the axles have two sets of arms that are identical to each other. The butyl chains are smaller than the -$(CH_2)_4$-COO_X side-arms (X = H or $SnCy_3$). The axles can enter into the cavity of the crown and form the interactions which were discussed above, as it can be inferred from the chemical shifts of the proton H_b and H_c. Other signals do not appear in the spectrum clearly, as the interaction between the crown and the axle interrupts them.

The NMR titrations were performed using 500µL of a 15DN38C10 solution in acetone-d_6 with an initial concentration of 5.12×10^{-4} M. To these solutions were added 0.1 equivalents of axle at a time and the NMR spectrum was recorded at each step. The H_b and H_c protons situated on the 15DN38C10 crown ether were monitored, and their shift upon adding increasing amounts of $BBI(Bu)_2[CH_2)_4\text{-}COOH]_2$ and $BBI(Bu)_2[(CH_2)_4\text{-}COO\text{-}SnCy_3]_2$ axles is shown in Figure III.7.a and III.7.b, respectively. The values of their association constants were evaluated using the BindFit software.[11,12]

Looking at H_b as an example, by plotting $\Delta\delta$ against the number of axle equivalents, the titration curves clearly show the saturation of the system, see in Figure III.8 the red and blue markers. Using the data collected during the experiment for Hb, we found an

association constant of 3.25 x 10^3 M^{-1} for the BBI$(Bu)_2$[$(CH_2)_4$-COOH]$_2$⊂15DN38C10 pseudorotaxane and 4.09 x 10^3 M^{-1} for the BBI$(Bu)_2$[$(CH_2)_4$-COO-SnCy_3]$_2$⊂15DN38C10 assembly. Similar results were obtained using the shift of the H_c proton.

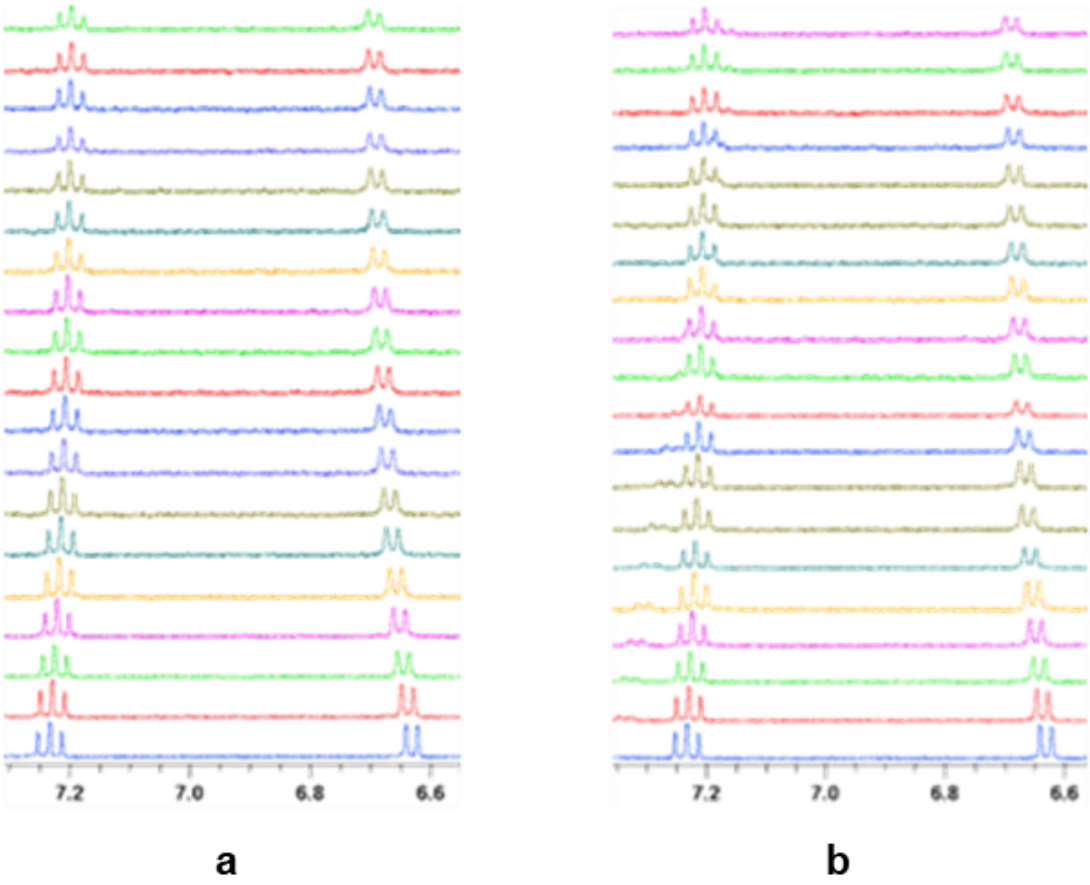

Figure III.7. a) The shift of the signals corresponding to the H_b protons in the case of BBI$(Bu)_2$[$(CH_2)_4$-COOH]$_2$⊂15DN38C10; b) the shift of the signals corresponding to the H_b protons in the case of BBI$(Bu)_2$[$(CH_2)_4$-COO-SnCy_3]$_2$⊂15DN38C10.

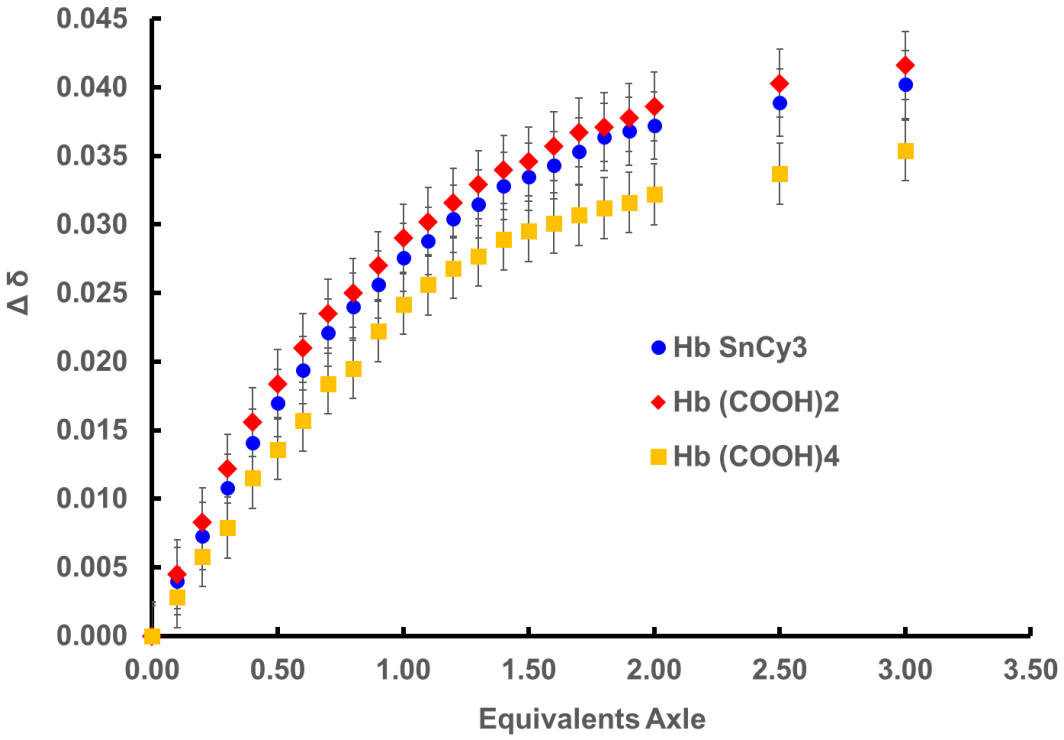

Figure III.8. Titration curves for the pseudorotaxane systems studied in this work.

Next, we investigated the interaction of the **I** and **J** axles with the same 15DN38C10 crown. The analysis of the $\{BBI[(CH_2)_4COOH)]_4\}(PF_6)_2 \subset$15DN38C10 system using the same method described above shows a similar behavior of this axle as observed with the "two-arms" examples. Using the same Bindfit software, the K_a value was determined to be 2.61 x 10^3 M^{-1}.

In contrast, $\{BBI[(CH_2)_4COOSnCy_3)]_4\}(PF_6)_2$ shows no significant interaction with the 15DN38C10 crown ether, presumably because the four -$COOSnCy_3$ termini of the side-arms are much larger than the cavity of the crown and it cannot form the pseudorotaxane.

Table III.1. lists the K_a values for the three architectures discussed here. As it can be seen, the $\{BBI(Bu)_2[(CH_2)_4\text{-}COO\text{-}SnCy_3]_2\}(PF_6)_2\subset$15DN38C10 species has the highest K_a value, followed by the dicarboxylic $\{BBI(Bu)_2[(CH_2)_4\text{-}COOH]_2\}(PF_6)_2\subset$15DN38C10 system, while the tetracarboxylic $\{BBI[(CH_2)_4COOH)]_4\}(PF_6)_2\subset$15DN38C10 pseudorotaxane shows the lowest K_a value.

This trend in the association constant values can be explained by the fact that $\{BBI(Bu)_2[(CH_2)_4\text{-}COO\text{-}SnCy_3]_2\}(PF_6)_2\subset$15DN38C10 has the two carboxylate donor groups coordinated to the bulky tricyclohexyltin $SnCy_3$ side-arms, thus preventing the dissociation of the pseudorotaxane interlocked species. In addition, besides the C2-H protons, there are no other acidic hydrogen atoms present that could participate in hydrogen bonding.

On another hand, the other two species, $\{BBI(Bu)_2[(CH_2)_4\text{-}COOH]_2\}(PF_6)_2\subset$15DN38C10 and $\{BBI[(CH_2)_4COOH)]_4\}(PF_6)_2\subset$15DN38C10 have two and four -COOH moieties, respectively, all available to enter in additional hydrogen bonding interactions. As the BBI core also have acidic hydrogens (the C2-H protons), hydrogen bonds between these and the -COOH regions might interfere with the formation of the interlocked species. When the two carboxylate-based examples are compared, the dicarboxylic species shows a higher K_a than the tetracarboxylic derivative (3.25×10^{-3} M^{-1} vs. 2.61×10^{-3} M^{-1}). In this case, the smaller value of the K_a could be explained by the fact that there are four carboxylic groups attached to the BBI core, thus providing more opportunities for hydrogen bonding.

Table III.1. Thermodynamic data for the pseudorotaxanes studied in this work.

Pseudorotaxane	K_a **(M^{-1})**
$\{BBI(Bu)_2[(CH_2)_4\text{-}COOH]_2\}(PF_6)_2\subset$15DN38C10	$(3.25 \pm 0.12) \times 10^3$
$\{BBI(Bu)_2[(CH_2)_4\text{-}COO\text{-}SnCy_3]_2\}(PF_6)_2\subset$15DN38C10	$(4.09 \pm 0.25) \times 10^3$
$\{BBI[(CH_2)_4COOH)]_4\}(PF_6)_2\subset$15DN38C10	$(2.61 \pm 0.56) \times 10^3$

III.4. Solid state studies

We were able to grow crystals suitable for X-ray diffraction studies only for the $\{BBI[(CH_2)_4COOH)]_4\}(PF_6)_2\subset$15DN38C10 pseudorotaxane; the other compounds produced poor diffracting microcrystalline materials. Single crystal X-ray diffraction studies (see Table III.2 for relevant crystal data and structure refinement details) performed on crystals grown from an acetone / diethyl ether system, revealed that the compound crystalizes in the triclinic space group P-1 and the asymmetric unit consists of one tetratopic axle, one crown ether species and a solvent molecule, with the final cell constants of a = 10.6162(3) Å, b = 13.1131(3) Å, c = 13.3143(3) Å, α = 102.510(2)°, β = 94.844(2)°, and γ = 98.423(2)°.

The structure is pictured in Figure III.9. The bond lengths and angles for this species fall within the normal values found in these compounds; a list of all bonds and angles are listed in Appendix A, along with other relevant crystallographic data. As it can be seen, the BBI^{2+} core is positioned inside the 15DN38C10 wheel, with the side-arms of the axle extending from the cavity of the crown ether, thus generating a starburst [2_4]pseudorotaxane, with all four side-arms of the BBI^{2+} moiety oriented away from the crown ether.

Table III.2. Crystal and refinement data for $\{BBI[(CH_2)_4COOH)]_4\}(PF_6)_2 \subset 15DN38C10$.

Crystal data	
Chemical formula	$C_{36}H_{44}O_{10} \cdot C_{28}H_{40}N_4O_8 \cdot 2\ PF_6 \cdot CH_2O_2$
M_r	1533.31
Crystal system, space group	Triclinic, *P-1*
Temperature (K)	100
a, *b*, *c* (Å)	10.6162(3), 13.1131(3), 13.3143(3)
α, β, γ (°)	102.510(2), 94.844(2), 98.423(2)
V (Å^3)	1776.98(8)
Z	1
Radiation type	Cu *K*α
μ (mm^{-1})	1.49
Crystal size (mm)	0.19 × 0.16 × 0.13
Data collection	
Absorption correction	Multi-scan *SADABS*
No. of measured, independent and observed [$I > 2\sigma(I)$] reflections	21595, 5310, 3879
R_{int}	0.066
θ_{max} (°)	61.3
$(\sin \theta/\lambda)_{max}$ (Å^{-1})	0.569
Refinement	
$R[F^2 > 2\sigma(F^2)]$, $wR(F^2)$, *S*	0.049, 0.134, 1.04
No. of reflections	5310
No. of parameters	482
H-atom treatment	H-atom parameters constrained
$\Delta\rho_{max}$, $\Delta\rho_{min}$ (e Å^{-3})	0.48, - 0.26

This pseudorotaxane architecture is being held in place by hydrogen bonding, π-π stacking, and several $[N - CH - N]^{+} \cdots O$ ion – dipole interactions. The C2-H atom of the BBI^{2+} group is involved in a hydrogen bond with one of the oxygen atom from the glycol chain of the crown ether; for this interaction, the O ⋯ H distance is 2.424 Å and the O – H – O angle is 144.65°. The π – π stacking interaction is characterized by a perpendicular distance between the BBI and naphthalene rings of 3.454 Å. These rings are positioned in a parallel displacement, at a 22.6° angle formed by the BBI centroid – centroid vector and the normal vector to the BBI plane. In addition, multiple $[N - CH - N]^{+} \cdots O$ ion – dipole interactions stabilize the pseudorotaxane structure, with C2 ⋯ O distances in the 3.246 – 3.783 Å interval. Table III.3 summarizes these interactions found from the crystallographic data.

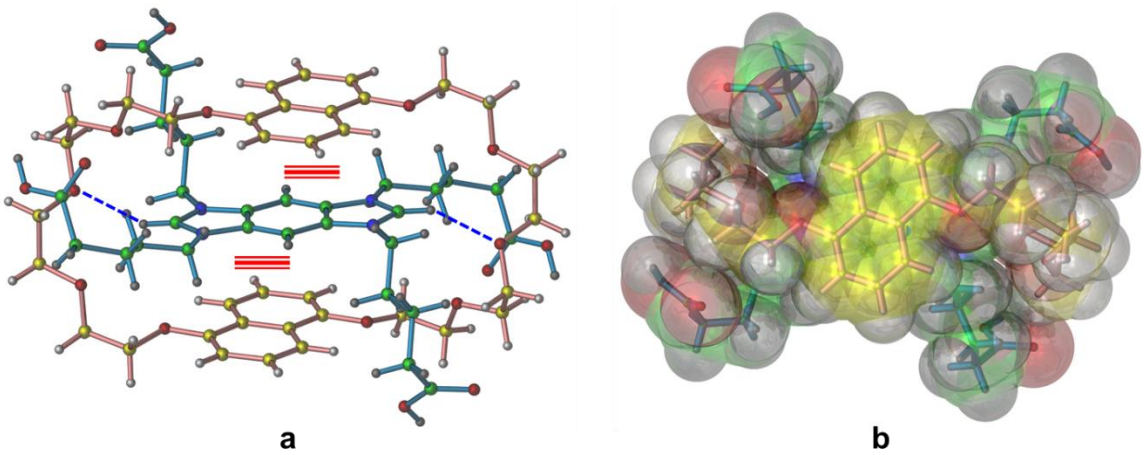

Figure III.9. The structure of the $\{BBI[(CH_2)_4COOH)]_4 \subset 15DN38C10\}^{2+}$ assembly: a) side view in ball and stick representation; the blue dashed lines show the H-bonding interactions, and the triple red lines the π-π stacking interactions; b) top view of the interlocked architecture as a space filling representation.

As suspected from our studies on the association constant of these species, all carboxylic groups on the BBI core are involved in multiple hydrogen bonding interactions. Figure III.10 shows how two opposite $–(CH_2)_4$-COOH side-arms form a double hydrogen bond. For this interaction, the O···H distance is 1.801 Å and the O – H – O angle is 166.53°. The other two side-arms of the axle are involved in a similar interaction with a solvent molecule. In this case, the O···H distance is 1.881 Å and the O – H – O angle is 147.86°. This collection of interactions leads to the formation of a supramolecular two dimensional array of $[2_4]$pseudorotaxanes.

Table III.3. Essential non-covalent interactions found in the molecular and crystal structure of $\{BBI[(CH_2)_4COOH)]_4\}(PF_6)_2 \subset 15DN38C10$.

Interactions holding together the pseudorotaxane assembly	
C2 – H ···O_{crown} distance	2.424 Å
C2 – H – O_{crown} angle	144.65°
π – π stacking, ⊥ distance[a]	3.454 Å
π – π stacking, β displacement angle[a]	22.6°
$[N – CH – N]^+$ ··· O distance interval	3.246 – 3.783 Å
Interactions holding together the supramolecular structure	
COOH double H-bond O···H distance	1.801 Å
COOH double H-bond O – H – O angle	166.53°
COOH – solvent O···H distance	1.881 Å
COOH – solvent O – H – O angle	147.86°

a) Calculated using Platon software.[13]

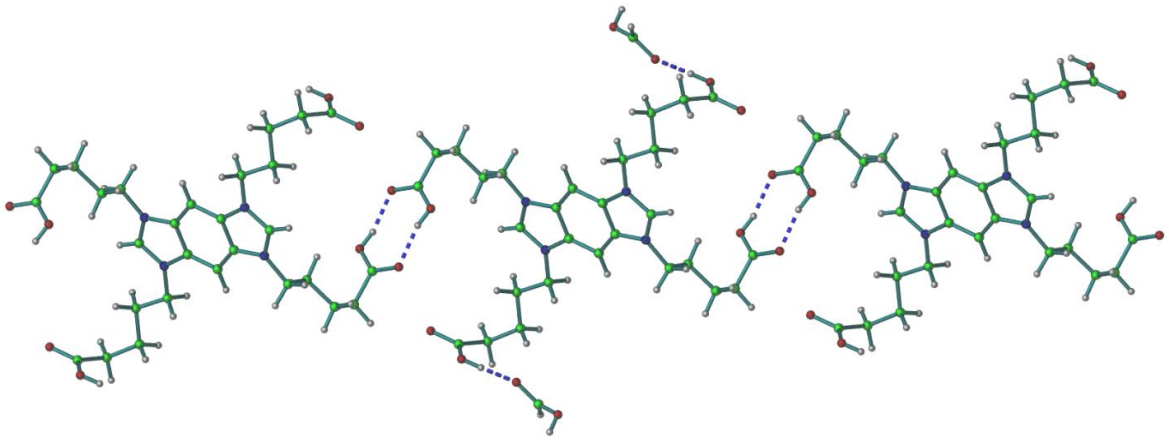

Figure III.10. The supramolecular association of the axle via hydrogen bonding interactions involving the carboxylic groups on the axle.

III.5. References

1. Pedersen, C. *J. Am. Chem. Soc*. **1967**, *89*, 7017.

2. Stoddart, J. F. *Chem. Soc. Rev*. **2009**, *38*, 1802.

3. Beves, J. E.; Blight, B. A.; Campbell, C. J.; Leigh, D. A.; McBurney, R. T.; *Angew. Chem. Int. Ed.* **2011**, *50*, 9260.

4. Champin, B.; Mobiana, P.; Sauvage, J. P.; *Chem. Soc. Rev*. **2007**, *36*, 358.

5. Cnossen, A.; Browne, W. R.; Feringa, B. L. *Top. Curr. Chem*. **2014**, *354*, 139.

6. Caballero, A.; Zapata, F.; Beer, P. D. *Coord. Chem. Rev*. **2013**, *257*, 2434.

7. Inthasot, A.; Tung, S. T.; Chiu, S. H.; *Acc. Chem. Res*. **2018**, *51*, 1324.

8. Vukotic, V. N.; Loeb, S. J.; *Chem. Soc. Rev*. **2012**, *41*, 5896.

9. Foster, M. W.; Mehl, B. T.; Treadwell, E. M.; Semeniuc, R. F.; Wheeler, K. A. *Chem. Commun.* **2019**, *55*, 1786.

10. Thordarson, P. *Chem. Soc. Rev*. **2011**, *40*, 1305.

11. Bindfit: http://supramolecular.org

12. Hibbert, B. D.; Thordarson, P. *Chem. Commun.* **2016**, *52*, 12792.

13. A. L. Spek, *Acta Cryst*. 2009, **D65**, 148.

IV. Conclusions and future work

We have described here the synthesis and characterization of several pseudorotaxanes, built on a benzobis(imidazolium) (BBI) core. This central unit can interact with crown ethers through a combination of hydrogen bonds, ion-dipole, and π-π stacking interactions to form starburst [2_4]pseudorotaxanes. This recognition motif allows the extension of four side-arms directly from the cavity of the crown ether, thus positioning the wheel component in a straddled orientation onto the axle, in sharp contrast to the classical shape showed by the regular [2_2]pseudorotaxanes.

In this study, axles with four side-arms which have a different number of donor sites were synthesized through multiple steps. We have prepared axles with two (ditopic) and four (tetratopic) carboxylate donor groups, respectively. The synthesis of the ditopic axles started with the addition of two nitro groups on a 1,3-dichlorobenzene body, which is the precursor to produce the desired benzobis(imidazolium) salts. Substitution of the chloro groups with two butyl moieties, followed by the formation of the BBI core followed. The next steps were the addition of two carboxylate-based side-arms to act as coordinating groups toward metallic centers (in our case a tricyclohexyltin(IV) group). The synthesis of the tetratopic axles used benzobis(imidazole) as starting material, to which four carboxylate side-arms were attached. In both cases, the reaction of the axles with tricyclohexyltin chloride in the presence of a base produced the desired tin substituted axles.

Once the axles were prepared, their interaction with the 15DN38C10 crown ether was studied. Four compounds were considered: the ditopic and tetratopic free carboxylic acids and their tin derivatives. Our studies suggest that the association constant depends on the nature of the axle termini (the carboxylic group is either free or coordinated to a metallic center), as well as on the number of such groups present on the central BBI unit (two vs. four carboxylic moieties).

As it has been shown, the $\{BBI(Bu)_2[(CH_2)_4\text{-}COO\text{-}SnCy_3]_2\}(PF_6)_2\subset$15DN38C10 species (where the carboxylic group is bonded to the tricyclohexyltin center) exhibited the highest K_a value, followed by the dicarboxylic $\{BBI(Bu)_2[(CH_2)_4\text{-}COOH]_2\}(PF_6)_2\subset$15DN38C10 system, while the tetracarboxylic $\{BBI[(CH_2)_4COOH)]_4\}(PF_6)_2\subset$15DN38C10 pseudorotaxane showed the lowest K_a value. The $\{BBI[(CH_2)_4COOSnCy_3)]_4\}(PF_6)_2$ axle did not present a significant interaction with the 15DN38C10 crown ether, as the four -$COOSnCy_3$ ends of the side-arms are much larger than the cavity of the crown, thus preventing the formation of the starburst $[2_4]$pseudorotaxane.

Solid state studies revealed that the structure of the $\{BBI[(CH_2)_4COOH)]_4\}(PF_6)_2\subset$ 15DN38C10 pseudorotaxane consists in the BBI core threaded into the cavity of the crown in a straddled orientation. Several carboxylate groups were identified participating in hydrogen bonding interactions, thus confirming our hypothesis that the association constant of these species is influenced by the nature of the groups appended on the BBI core and by their number.

Future work would include the characterization of the synthesized pseudorotaxanes using other methods of investigations, to determine if the presence of the crown ether has an impact on the photophysical properties of the BBI core. Another development of this chemistry is to attach to the sidearms of the axle other metallic centers, such as $[(bipy)Re(CO)_3]^+$ and $[(bipy)_2Ru]^{2+}$, both known for their interesting photophysical properties. Attaching to the BBI core other sidearms having a different donor set (e.g. a bis(pyrazolyl)methane unit instead of the carboxylate donor) would also expand the family of these species.

Another development would be the synthesis and characterization of MORFs. This goal could be achieved by using other metallic centers that would allow the expansion of the pseudorotaxane in multiple directions, as opposed to forming discrete compounds, as described here.

APPENDIX A

Crystal Structure Report for $\{BBI[(CH_2)_4COOH)]_4\}(PF_6)_2 \subset 15DN38C10$.

A specimen of $C_{65}H_{86}F_{12}N_4O_{20}P_2$, approximate dimensions 0.130 mm x 0.160 mm x 0.190 mm, was used for the X-ray crystallographic analysis. The X-ray intensity data were measured (λ = 1.54178 Å). A total of 6528 frames were collected. The total exposure time was 18.13 hours. The frames were integrated with the Bruker SAINT software package using a narrow-frame algorithm. The integration of the data using a triclinic unit cell yielded a total of 21595 reflections to a maximum θ angle of 61.30° (0.88 Å resolution), of which 5310 were independent (average redundancy 4.067, completeness = 96.9%, R_{int} = 6.57%, R_{sig} = 4.77%) and 3879 (73.05%) were greater than $2\sigma(F^2)$. The final cell constants of $\underline{a}$ = 10.6162(3) Å, $\underline{b}$ = 13.1131(3) Å, $\underline{c}$ = 13.3143(3) Å, α = 102.510(2)°, β = 94.844(2)°, γ = 98.423(2)°, volume = 1776.98(8) $Å^3$, are based upon the refinement of the XYZ-centroids of 119 reflections above 20 σ(I) with 6.944° < 2θ < 90.48°. Data were corrected for absorption effects using the Multi-Scan method (SADABS). The ratio of minimum to maximum apparent transmission was 0.882.

The structure was solved and refined using the Bruker SHELXTL Software Package, using the space group P -1, with Z = 1 for the formula unit, $C_{65}H_{86}F_{12}N_4O_{20}P_2$. The final anisotropic full-matrix least-squares refinement on F^2 with 482 variables converged at R1 = 4.90%, for the observed data and wR2 = 13.35% for all data. The goodness-of-fit was 1.040. The largest peak in the final difference electron density synthesis was 0.483 $e^-/Å^3$ and the largest hole was -0.256 $e^-/Å^3$ with an RMS deviation of 0.057 $e^-/Å^3$. On the basis of the final model, the calculated density was 1.433 g/cm^3 and F(000), 802 e^-.

Table 1. Crystal and refinement data for {BBI[$(CH_2)_4COOH$)]$_4$}$(PF_6)_2$⊂15DN38C10.

Crystal data	
Chemical formula	$C_{36}H_{44}O_{10} \cdot C_{28}H_{40}N_4O_8 \cdot 2\ PF_6 \cdot CH_2O_2$
M_r	1533.31
Crystal system, space group	Triclinic, *P-1*
Temperature (K)	100
a, *b*, *c* (Å)	10.6162(3), 13.1131(3), 13.3143(3)
α, β, γ (°)	102.510(2), 94.844(2), 98.423(2)
V (Å^3)	1776.98(8)
Z	1
Radiation type	Cu *K*α
μ (mm^{-1})	1.49
Crystal size (mm)	0.19 × 0.16 × 0.13
Data collection	
Absorption correction	Multi-scan *SADABS*
No. of measured, independent and observed [$I > 2\sigma(I)$] reflections	21595, 5310, 3879
R_{int}	0.066
θ_{max} (°)	61.3
$(\sin\theta/\lambda)_{max}$ (Å^{-1})	0.569
Refinement	
$R[F^2 > 2\sigma(F^2)]$, $wR(F^2)$, *S*	0.049, 0.134, 1.04
No. of reflections	5310
No. of parameters	482
H-atom treatment	H-atom parameters constrained
$\Delta\rho_{max}$, $\Delta\rho_{min}$ (e Å^{-3})	0.48, - 0.26

Table 2. Bond lengths (Å) for {BBI[$(CH_2)_4COOH$)]$_4$}$(PF_6)_2$⊂15DN38C10.

O1-C1	1.274(5)	O1-H1	0.84
O2-C1	1.263(5)	O3-C14	1.270(4)
O3-H3	0.84	O4-C14	1.265(4)
O5-C15	1.422(4)	O5-C16	1.429(4)
O6-C18	1.368(4)	O6-C17	1.429(4)
O7-C27	1.380(4)	O7-C28	1.435(4)
O8-C29	1.420(4)	O8-C30	1.432(3)
O9-C32	1.424(4)	O9-C31	1.433(4)
N1-C7	1.326(4)	N1-C6	1.395(4)
N1-C5	1.472(4)	N2-C7	1.332(4)
N2-C8	1.400(4)	N2-C10	1.471(4)
C1-C2	1.500(5)	C2-C3	1.529(5)
C2-H2A	0.99	C2-H2AB	0.99
C3-C4	1.526(4)	C3-H3A	0.99
C3-H3AB	0.99	C4-C5	1.511(4)
C4-H4A	0.99	C4-H4AB	0.99
C5-H5A	0.99	C5-H5AB	0.99
C6-C9#1	1.388(4)	C6-C8	1.410(4)
C7-H7	0.95	C8-C9	1.377(4)
C9-H9	0.95	C10-C11	1.519(4)
C10-H10A	0.99	C10-H10B	0.99
C11-C12	1.522(4)	C11-H11A	0.99
C11-H11B	0.99	C12-C13	1.545(4)
C12-H12A	0.99	C12-H12B	0.99
C13-C14	1.491(5)	C13-H13A	0.99
C13-H13B	0.99	C15-C32#2	1.505(5)
C15-H15A	0.99	C15-H15B	0.99
C16-C17	1.490(4)	C16-H16A	0.99
C16-H16B	0.99	C17-H17A	0.99
C17-H17B	0.99	C18-C19	1.364(4)
C18-C23	1.434(4)	C19-C20	1.412(4)
C19-H19	0.95	C20-C21	1.364(4)
C20-H20	0.95	C21-C22	1.418(4)
C21-H21	0.95	C22-C23	1.408(4)

C22-C27	1.429(4)	C23-C24	1.424(4)
C24-C25	1.361(5)	C24-H24	0.95
C25-C26	1.407(5)	C25-H25	0.95
C26-C27	1.366(4)	C26-H26	0.95
C28-C29	1.496(4)	C28-H28A	0.99
C28-H28B	0.99	C29-H29A	0.99
C29-H29B	0.99	C30-C31	1.493(4)
C30-H30A	0.99	C30-H30B	0.99
C31-H31A	0.99	C31-H31B	0.99
C32-H32A	0.99	C32-H32B	0.99
P1-F5	1.576(2)	P1-F1	1.585(2)
P1-F2	1.585(2)	P1-F3	1.586(2)
P1-F4	1.589(2)	P1-F6	1.590(2)
O10-C33	1.204(10)	O10-H10	0.84
O11-C33	1.232(9)	C33-H33A	0.95

Table 3. Bond angles (°) for $\{BBI[(CH_2)_4COOH)]_4\}(PF_6)_2 \subset 15DN38C10$.

C1-O1-H1	109.5	C14-O3-H3	109.5
C15-O5-C16	111.7(2)	C18-O6-C17	117.3(2)
C27-O7-C28	117.5(2)	C29-O8-C30	113.7(2)
C32-O9-C31	112.5(2)	C7-N1-C6	108.8(2)
C7-N1-C5	124.7(2)	C6-N1-C5	126.4(2)
C7-N2-C8	108.3(2)	C7-N2-C10	128.0(3)
C8-N2-C10	123.7(2)	O2-C1-O1	124.6(4)
O2-C1-C2	118.0(4)	O1-C1-C2	117.5(4)
C1-C2-C3	110.7(3)	C1-C2-H2A	109.5
C3-C2-H2A	109.5	C1-C2-H2AB	109.5
C3-C2-H2AB	109.5	H2A-C2-H2AB	108.1
C4-C3-C2	113.0(3)	C4-C3-H3A	109.0
C2-C3-H3A	109.0	C4-C3-H3AB	109.0
C2-C3-H3AB	109.0	H3A-C3-H3AB	107.8
C5-C4-C3	110.6(3)	C5-C4-H4A	109.5
C3-C4-H4A	109.5	C5-C4-H4AB	109.5
C3-C4-H4AB	109.5	H4A-C4-H4AB	108.1
N1-C5-C4	111.3(2)	N1-C5-H5A	109.4

C4-C5-H5A	109.4	N1-C5-H5AB	109.4
C4-C5-H5AB	109.4	H5A-C5-H5AB	108.0
C9#1-C6-N1	130.7(3)	C9#1-C6-C8	123.2(3)
N1-C6-C8	106.1(2)	N1-C7-N2	110.7(3)
N1-C7-H7	124.7	N2-C7-H7	124.7
C9-C8-N2	129.7(3)	C9-C8-C6	124.2(3)
N2-C8-C6	106.1(2)	C8-C9-C6#1	112.6(3)
C8-C9-H9	123.7	C6#1-C9-H9	123.7
N2-C10-C11	113.8(2)	N2-C10-H10A	108.8
C11-C10-H10A	108.8	N2-C10-H10B	108.8
C11-C10-H10B	108.8	H10A-C10-H10B	107.7
C10-C11-C12	109.6(3)	C10-C11-H11A	109.8
C12-C11-H11A	109.8	C10-C11-H11B	109.8
C12-C11-H11B	109.8	H11A-C11-H11B	108.2
C11-C12-C13	112.2(3)	C11-C12-H12A	109.2
C13-C12-H12A	109.2	C11-C12-H12B	109.2
C13-C12-H12B	109.2	H12A-C12-H12B	107.9
C14-C13-C12	113.1(3)	C14-C13-H13A	109.0
C12-C13-H13A	109.0	C14-C13-H13B	109.0
C12-C13-H13B	109.0	H13A-C13-H13B	107.8
O4-C14-O3	119.6(3)	O4-C14-C13	118.5(3)
O3-C14-C13	121.9(3)	O5-C15-C32#2	109.0(3)
O5-C15-H15A	109.9	C32#2-C15-H15A	109.9
O5-C15-H15B	109.9	C32#2-C15-H15B	109.9
H15A-C15-H15B	108.3	O5-C16-C17	109.8(2)
O5-C16-H16A	109.7	C17-C16-H16A	109.7
O5-C16-H16B	109.7	C17-C16-H16B	109.7
H16A-C16-H16B	108.2	O6-C17-C16	107.8(3)
O6-C17-H17A	110.1	C16-C17-H17A	110.1
O6-C17-H17B	110.1	C16-C17-H17B	110.1
H17A-C17-H17B	108.5	C19-C18-O6	125.3(3)
C19-C18-C23	120.9(3)	O6-C18-C23	113.8(3)
C18-C19-C20	119.8(3)	C18-C19-H19	120.1
C20-C19-H19	120.1	C21-C20-C19	121.1(3)
C21-C20-H20	119.5	C19-C20-H20	119.5
C20-C21-C22	120.1(3)	C20-C21-H21	120.0

C22-C21-H21	120.0	C23-C22-C21	119.8(3)
C23-C22-C27	117.6(3)	C21-C22-C27	122.6(3)
C22-C23-C24	120.3(3)	C22-C23-C18	118.3(3)
C24-C23-C18	121.4(3)	C25-C24-C23	119.5(3)
C25-C24-H24	120.2	C23-C24-H24	120.2
C24-C25-C26	121.6(3)	C24-C25-H25	119.2
C26-C25-H25	119.2	C27-C26-C25	119.3(3)
C27-C26-H26	120.3	C25-C26-H26	120.3
C26-C27-O7	124.4(3)	C26-C27-C22	121.6(3)
O7-C27-C22	114.0(3)	O7-C28-C29	106.7(2)
O7-C28-H28A	110.4	C29-C28-H28A	110.4
O7-C28-H28B	110.4	C29-C28-H28B	110.4
H28A-C28-H28B	108.6	O8-C29-C28	107.8(3)
O8-C29-H29A	110.1	C28-C29-H29A	110.1
O8-C29-H29B	110.1	C28-C29-H29B	110.1
H29A-C29-H29B	108.5	O8-C30-C31	107.7(2)
O8-C30-H30A	110.2	C31-C30-H30A	110.2
O8-C30-H30B	110.2	C31-C30-H30B	110.2
H30A-C30-H30B	108.5	O9-C31-C30	108.2(2)
O9-C31-H31A	110.1	C30-C31-H31A	110.1
O9-C31-H31B	110.1	C30-C31-H31B	110.1
H31A-C31-H31B	108.4	O9-C32-C15#2	113.8(2)
O9-C32-H32A	108.8	C15#2-C32-H32A	108.8
O9-C32-H32B	108.8	C15#2-C32-H32B	108.8
H32A-C32-H32B	107.7	F5-P1-F1	89.80(16)
F5-P1-F2	179.73(15)	F1-P1-F2	90.07(15)
F5-P1-F3	89.45(14)	F1-P1-F3	90.88(13)
F2-P1-F3	90.79(13)	F5-P1-F4	90.02(17)
F1-P1-F4	179.03(15)	F2-P1-F4	90.11(16)
F3-P1-F4	90.08(12)	F5-P1-F6	90.79(14)
F1-P1-F6	89.21(13)	F2-P1-F6	88.98(13)
F3-P1-F6	179.75(15)	F4-P1-F6	89.84(12)
C33-O10-H10	109.5	O10-C33-O11	130.2(8)
O10-C33-H33A	114.9	O11-C33-H33A	114.9

Table 4. Torsion angles (°) for {BBI[$(CH_2)_4COOH$)]$_4$}$(PF_6)_2$⊂15DN38C10.

O2-C1-C2-C3	-74.5(4)	O1-C1-C2-C3	105.2(4)
C1-C2-C3-C4	-63.1(4)	C2-C3-C4-C5	-178.7(3)
C7-N1-C5-C4	103.8(3)	C6-N1-C5-C4	-71.6(4)
C3-C4-C5-N1	-172.2(3)	C7-N1-C6-C9#1	-179.6(3)
C5-N1-C6-C9#1	-3.5(5)	C7-N1-C6-C8	0.1(3)
C5-N1-C6-C8	176.1(3)	C6-N1-C7-N2	0.0(3)
C5-N1-C7-N2	-176.2(2)	C8-N2-C7-N1	0.0(3)
C10-N2-C7-N1	178.7(3)	C7-N2-C8-C9	-179.6(3)
C10-N2-C8-C9	1.6(5)	C7-N2-C8-C6	0.1(3)
C10-N2-C8-C6	-178.7(3)	C9#1-C6-C8-C9	-0.8(5)
N1-C6-C8-C9	179.6(3)	C9#1-C6-C8-N2	179.6(3)
N1-C6-C8-N2	-0.1(3)	N2-C8-C9-C6#1	-179.7(3)
C6-C8-C9-C6#1	0.7(5)	C7-N2-C10-C11	-10.0(4)
C8-N2-C10-C11	168.5(3)	N2-C10-C11-C12	-169.6(3)
C10-C11-C12-C13	174.5(3)	C11-C12-C13-C14	-64.3(4)
C12-C13-C14-O4	130.0(3)	C12-C13-C14-O3	-49.8(4)
C16-O5-C15-C32#2	-165.4(3)	C15-O5-C16-C17	-170.5(3)
C18-O6-C17-C16	-171.8(2)	O5-C16-C17-O6	-63.2(3)
C17-O6-C18-C19	-8.0(4)	C17-O6-C18-C23	172.3(2)
O6-C18-C19-C20	179.8(3)	C23-C18-C19-C20	-0.5(4)
C18-C19-C20-C21	0.5(4)	C19-C20-C21-C22	-0.1(4)
C20-C21-C22-C23	-0.3(4)	C20-C21-C22-C27	-179.5(3)
C21-C22-C23-C24	-178.8(3)	C27-C22-C23-C24	0.5(4)
C21-C22-C23-C18	0.3(4)	C27-C22-C23-C18	179.6(3)
C19-C18-C23-C22	0.0(4)	O6-C18-C23-C22	179.8(2)
C19-C18-C23-C24	179.2(3)	O6-C18-C23-C24	-1.1(4)
C22-C23-C24-C25	-0.3(4)	C18-C23-C24-C25	-179.4(3)
C23-C24-C25-C26	0.0(5)	C24-C25-C26-C27	0.1(5)
C25-C26-C27-O7	-179.2(3)	C25-C26-C27-C22	0.1(5)
C28-O7-C27-C26	-12.4(4)	C28-O7-C27-C22	168.3(3)
C23-C22-C27-C26	-0.4(4)	C21-C22-C27-C26	178.9(3)
C23-C22-C27-O7	179.0(2)	C21-C22-C27-O7	-1.8(4)
C27-O7-C28-C29	173.8(2)	C30-O8-C29-C28	-180.0(2)
O7-C28-C29-O8	-72.3(3)	C29-O8-C30-C31	177.8(2)

C32-O9-C31-C30	159.1(2)	O8-C30-C31-O9	68.5(3)
C31-O9-C32-C15#2	68.2(3)		

Symmetry transformations used to generate equivalent atoms:

#1	-x, -y, -z
#2	-x+2, -y, -z